

Fe XXV and Fe XXVI Diagnostics of the Black Hole and Accretion Disk in Active Galaxies: Chandra Time-Resolved Spectroscopy of NGC 7314

Tahir Yaqoob^{a b}, Ian M. George^{b c}, Timothy R. Kallman^b, Urmila Padmanabhan^a, Kimberly A. Weaver^b, T. Jane Turner^{b c}

^a*Department of Physics and Astronomy, Johns Hopkins University, Baltimore, MD 21218.*

^b*Laboratory for High Energy Astrophysics, NASA/Goddard Space Flight Center, Greenbelt, MD 20771.*

^c*Joint Center for Astrophysics, University of Maryland, Baltimore County, 1000 Hilltop Circle, Baltimore, MD 21250.*

Abstract

We report the detection of Fe XXV and Fe XXVI $K\alpha$ emission lines from a *Chandra* High Energy Grating Spectrometer (*HETGS*) observation of the narrow-line Seyfert 1 galaxy NGC 7314, made simultaneously with *RXTE*. The lines are redshifted ($cz \sim 1500 \text{ km s}^{-1}$) relative to the systemic velocity and unresolved by the gratings. We argue that the lines originate in a near face-on ($< 7^\circ$) disk having a radial line emissivity flatter than r^{-2} . Line emission from ionization states of Fe in the range $\sim \text{Fe I a}$ up to Fe XXVI is observed. The ionization balance of Fe responds to continuum variations on timescales less than 12.5 ks, supporting an origin of the lines close to the X-ray source. We present additional, detailed diagnostics from this rich data set. These results identify NGC 7314 as a key source to study in the future if we are to pursue reverberation mapping of space-time near black-hole event horizons. This is because it is first necessary to understand the ionization structure of accretion disks and the relation between the X-ray continuum and Fe $K\alpha$ line emission. However, we also describe how our results are suggestive of a means of measuring black-hole spin without a knowledge of the relation between the continuum and line emission. Finally, these data emphasize that one *can* study strong gravity with narrow (as opposed to very broad) disk lines. In fact narrow lines offer higher precision, given sufficient energy resolution.

Keywords: black hole physics – accretion disks – galaxies: active – line: profile – X-rays: galaxies – X-rays: individual (NGC 7314)

Accepted for Publication in the Astrophysical Journal 20 June 2003. Submitted 22 Jan 2003

1. INTRODUCTION

At least part of the Fe $K\alpha$ fluorescent emission line in active galactic nuclei (AGN) is believed to originate in a relativistic accretion disk around a black hole (e.g. see reviews by Fabian *et al.* 2000; Reynolds & Nowak 2003). In order to ultimately use the Fe $K\alpha$ lines to probe the space-time around a black hole, it has been recognized that it will be necessary to understand the complex ionization physics of the accretion disk (e.g. Nayakshin & Kallman 2001; Ballantyne, Ross, & Fabian 2001; Ballantyne & Ross 2002). In particular, we must understand the relation between the continuum and line emission. The basic observational data to build such an understanding is sparse. One needs to identify sources with rapidly variable line and continuum

emission, in which the dynamic range of the continuum variability is large. Once the emission-line variability is firmly established, the ground-work can be prepared for future missions to use these sources for time-resolved spectroscopy to probe shorter and shorter timescales, with higher spectral resolution.

Even in the first study of the Fe $K\alpha$ line emission in a sample of type 1 AGN (Nandra *et al.* 1997), the variety in the shape and width of the Fe $K\alpha$ line was pointed out. The range in width has been confirmed by subsequent studies (e.g. Lubiński and Zdziarski 2001; Yaqoob *et al.* 2002; Perola *et al.* 2002; Reeves 2002; Yaqoob & Padmanabhan 2002). We have now observed Fe $K\alpha$ lines with FWHM less than 40 eV, to more than a couple of keV. It has been traditional to associate ‘narrow’ Fe $K\alpha$ lines with an origin in distant

matter, at least several thousand gravitational radii from the black hole (e.g. the optical broad-line region (BLR), the putative obscuring torus, or the optical narrow-line region (NLR)). However, Petrucci *et al.* (2002) recently reported a *variable*, narrow Fe K α line in Mkn 841, supporting an accretion-disk origin. In addition, it has been pointed out that Fe K α lines which appear to be narrow even with the highest spectral resolution instruments currently available (the *Chandra* gratings), may have a significant contribution from the accretion disk (Lee *et al.* 2002; Yaqoob & Padmanabhan 2002). While such lines may be interpreted in terms of a truncated disk (e.g. Done, Madejski, & Życki 2000), they could be due to a flat radial line emissivity (i.e. intensity per unit area falling off with radius more slowly than r^{-2}).

In this paper we report on the results of a high spectral resolution *Chandra* grating observation of the narrow emission-line Seyfert 1 galaxy (NELG) NGC 7314 in which we detect Fe K α emission from not only the low ionization states of Fe (Fe XVII or lower), but also from redshifted He-like, and H-like Fe. We find that the ionization balance of Fe responds to rapid continuum variations, ruling out a distant-matter origin for the high ionization-state lines. We are able to use these line diagnostics to infer quantitative, new information about the black-hole/accretion disk system in NGC 7314, opening up similar possibilities for other AGN.

NGC 7314 is known for its rapid, large amplitude X-ray variability (Turner 1987; Yaqoob *et al.* 1996; Branduardi-Raymont *et al.* 2002). The luminosity can change by a factor of ~ 2 on a timescale of hundreds of seconds and by a factor of ~ 4 in thousands of seconds. The luminosity itself is fairly low: even at the peaks of the largest flares, the 2–10 keV luminosity is only $\sim 2 \times 10^{42}$ ergs s $^{-1}$ (we assume $H_0 = 70$ km s $^{-1}$ Mpc $^{-1}$ and $q_0 = 0$ throughout). It is well known that the least luminous Seyfert 1 galaxies are the most variable (e.g. Green, McHardy, & Lehto 1993; Turner *et al.* 1999) and measurements of the mass of the putative central black hole yield a correspondingly small value of $\sim 5 \times 10^6 M_\odot$ (Padovani & Rafanelli 1988; Schulz, Knake, & Schmidt-Kaler 1994). NGC 7314 was also one of the first AGN in which rapid variability of the Fe-K emission complex was found (Yaqoob *et al.* 1996). However, the limited spectral resolution of *ASCA*

restricted the diagnostics that could be made using this variability. The main result was that the emission in the red and blue wings of the line profile responded to the continuum intensity, whilst the core emission at 6.4 keV did not respond. Thus, we observed NGC 7314 with the highest spectral resolution available in the Fe-K band, using the *Chandra* gratings, in order to elucidate the nature of the line emission and its variability. The observation was made simultaneously with *RXTE* in order to measure the hard X-ray continuum as well, since it can provide additional constraints on the accretion disk.

In this paper we adopt $z = 0.004760$ for the redshift of NGC 7314, which was obtained from H I measurements (Mathewson & Ford 1996). We shall see that the *Chandra* data are sensitive to uncertainties in z of 0.00022, but this is larger than the uncertainty quoted by Mathewson & Ford (1996), of ± 0.000033 . The Galactic column density along the line-of-sight to NGC 7314 is small, and we use the value 1.46×10^{20} cm $^{-2}$ (Dickey & Lockman, 1990) throughout this paper.

The paper is organized as follows. In §2 we describe the observations, data, and methods of analysis. In §3 we present the results of high spectral resolution, time-resolved spectroscopy of the Fe-K region, revealing a wide and variable mix of ionization states of Fe. In §4 we describe how the measurement of relativistic effects from the X-ray emission-lines can be used to constrain the structure of the accretion disk. Then in §5 we discuss how simultaneous *RXTE* data add further constraints on the accretion disk. In §6 we discuss the implications of our results for AGN in general, and how future instrumentation could be used to advance our knowledge further. Finally, in §7 we summarize our results.

2. OBSERVATIONS AND DATA

We observed NGC 7314 with *Chandra* in July 2002, simultaneously with *RXTE*. The *Chandra* observation was made in two parts, on July 19, from UT 04:26:00 to UT 12:45:44, and on July 20, from UT 03:18:16 to UT 22:42:19. The *RXTE* observation was made from July 19 UT 04:39:21 to July 22 UT 16:26:34.

For this study the *Chandra* observation was made with the High-Energy Transmission Grating (or *HETGS* – Markert, *et al.* 1995) in the fo-

cal plane of the High Resolution Mirror Assembly. The *Chandra* HETGS affords the best spectral resolution in the $\sim 6-7$ keV Fe-K band currently available (~ 39 eV, or 1860 km s^{-1} FWHM at 6.4 keV). HETGS consists of two grating assemblies, a High-Energy Grating (HEG) and a Medium-Energy Grating (MEG), and it is the HEG which achieves this spectral resolution. The MEG spectral resolution is only half that of the HEG. The HEG also has higher effective area in the Fe-K band, so our study will focus principally on the HEG data. The HEG and MEG energy bands are 0.4–10 keV and 0.7–10 keV respectively, but the effective area falls off rapidly with energy near both ends of each bandpass. The *Chandra* data were processed with version 6.8.0 of the processing software, CALDB version 2.15 was used, and the telescope responses made using `ciao 2.1.3`¹. Otherwise, HEG and MEG lightcurves and spectra were made exactly as described in Yaqoob *et al.* (2003). We used only the first orders of the grating data (combining the positive and negative arms). The zeroth order data were piled up and the higher orders contain much fewer counts than the first order. The mean count rates (in the full energy band of each grating), over the entire *Chandra* observation were 0.1965 ± 0.0014 ct/s and 0.3532 ± 0.0019 ct/s for HEG and MEG respectively. HEG and MEG spectra extracted over the entire observation, resulted in a net exposure time of 97.248 ks. Background was not subtracted since it is negligible above ~ 0.6 keV (see also §3 and Fig. 2[a]).

The *RXTE* PCA data were reduced using methods described in Weaver, Krolik, & Pier (1998), except that we used a later version of the spectral response matrix generator (V 8.0) and the latest version of background model ('L7_240_FAINT') released in February 2002, with `ftools v5.2`. Only data from layer 1 were used. Of the five PCUs of the PCA, fewer were operated later in the mission than earlier, and we obtained useful data only from PCU0 and PCU2. We extracted background-subtracted lightcurves and spectra from each PCU separately. For weak sources, such as AGN, the PCA spectra may be unreliable above ~ 15 keV, when the background-subtraction systematics become too large. The usable low-energy limit of the spectra is ~ 3 keV, below which the instrument response is too uncer-

tain. For spectra extracted over the entire *RXTE* observation (which continued beyond the *Chandra* observation), the exposure time was 82.128 ks (each PCU) and the mean 3–15 keV background-subtracted count rates were 3.415 ± 0.015 ct/s and 2.994 ± 0.011 ct/s per PCU, for PCU0 and PCU2 respectively. However, in this paper we will use only the *RXTE* data which overlapped with *Chandra* (see §2.2).

2.1. *Chandra* and *RXTE* Cross-Calibration

Model-fitting cannot be performed on contemporaneous *Chandra* and *RXTE* data simply by spectral fitting to the spectra from different instruments simultaneously. This is because the effective area of the *RXTE* PCA is so much larger than the *Chandra* HETGS that the former will bias the fits (PCA:HEG ratio is > 40 per PCU at 6.4 keV). Also, the spectral resolution of the PCA is more than a factor of 30 worse than the HEG in the Fe-K band. Therefore we will take the approach of spectral fitting data from the different instruments independently and use any line emission measurements from the *Chandra* HETGS as fixed components of any model used to perform spectral fitting on the PCA data. In the case of complex line emission, all the parameters measured from the *Chandra* data have to be fixed, otherwise the PCA spectral fits become unstable, as the PCA can confuse line emission and continuum due to the poor spectral resolution. In order to execute this approach we must know at least the cross-normalization between the *Chandra* and *RXTE* instruments. This is because all line intensities measured by *Chandra* have to be adjusted before they can be applied to the PCA data.

Although cross-calibration studies have shown that *Chandra* fluxes generally agree well with other missions², it is known that in the 3–10 keV band PCA fluxes are systematically higher than *ASCA* and *BeppoSAX* fluxes³. However, these PCA cross-calibration results are out of date since new background-subtraction and calibration for PCA data have since been introduced. Therefore we studied a simultaneous *Chandra* / *RXTE* observation of the Seyfert 1 galaxy Fairall 9, observed in 2001, September 11. These data sets are available from the public archives and were

¹http://asc.harvard.edu/ciao2.1/documents_threads.html

²<http://space.mit.edu/ASC/calib/hetgcal.html>

³ASCA GOF calibration memo at

http://heasarc.gsfc.nasa.gov/docs/asca/calibration/3c273_results.html

selected because in these observations the source had an X-ray spectrum which was a simple power law in the 0.6–15 keV band (after accounting for Galactic absorption), no spectral features apart from an Fe K α line in the 6–7 keV band, and no X-ray variability was detected. We measured the excess variance (e.g. see Turner *et al.* 1999) from the *Chandra* *HETGS* data (0.8–7 keV for HEG, 0.6–5 keV for MEG, binned at 128 s) to be $(1.5 \pm 6.5) \times 10^{-4}$.

PCU0 did not yield any useful data for the Fairall 9 observation so we used only PCU2 for the cross-calibration of flux, extracting a spectrum over the entire observation (yielding an exposure time of 66.928 ks). Since we will only use the HEG data for studying the Fe-K region in NGC 7314, we extracted a HEG first-order spectrum over the entire observation of Fairall 9 (yielding an exposure time of 78.893 ks). We fitted the 3–9 keV HEG and PCA spectra independently with a simple power-law model plus Gaussian emission line and obtained good fits for both. The energy range used is accessible to both instruments. The HEG spectrum gave a photon index which was steeper by ~ 0.1 than that obtained from the PCA spectrum. We then measured the 6–7 keV fluxes from the best-fitting models and found that line intensities measured by the *Chandra* HEG must be increased by 14.7% if they are to be applied to PCA PCU2 data. Also, we compared the normalization of PCU0 with PCU2 using our NGC 7314 data and found a 3% difference in the normalization between the two PCUs. Therefore, if we are using combined PCU0 and PCU2 spectra with equal weighting, *Chandra* HEG line intensities must be increased by 13.0% and we adopted this latter value for cross-normalization of emission lines in the Fe-K region. Note that there have been no changes in the calibration of either the HEG or PCA over the period between the Fairall 9 and NGC 7314 observations that would significantly affect this result.

2.2. Lightcurves and Intensity-Selected Spectra

Fig. 1 shows the *Chandra* *HETGS* and *RXTE* PCA lightcurves binned at 128 s. The *HETGS* lightcurve was made from combined 0.8–7 keV HEG and MEG data (first order only). The PCA lightcurve was made from PCU2 only, in the 3–13 keV band (the upper energy was chosen to be

less than 15 keV as an extra precaution against background contamination). It can be seen that the *Chandra* lightcurve covers ~ 2 days, with a large gap of $\sim 1/3$ day starting ~ 30 ks into the observation. The PCA lightcurve intermittently covers all of the period of the *Chandra* observation. The large amplitude, rapid variability which is characteristic of NGC 7314 is again evident in the lightcurves. Variations by a factor ~ 2 on timescales of hundreds of seconds occur frequently, and a very large amplitude drop in flux is seen toward the end of the observations, when the flux dropped by a factor ~ 4 in ~ 3 ks.

We extracted intensity-selected HEG, MEG, and PCA spectra such that ‘low-state’ spectra were made from time intervals during which the 0.8–7 keV first order *HETGS* (i.e. HEG plus MEG) count rate was less than 0.60 ct/s (dotted line in Fig. 1), and ‘high-state’ spectra were made from intervals with > 0.61 *HETGS* first-order ct/s. This resulted in a low-state spectrum which had 0.1580 ± 0.0016 HEG ct/s, 0.2811 ± 0.0022 MEG ct/s, and a net exposure time of 59.440 ks. The corresponding values for the high state were 0.2610 ± 0.0028 HEG ct/s, 0.4796 ± 0.0038 MEG ct/s, and 32.869 ks net exposure time. Since the overlap of *Chandra* and *RXTE* is not perfect, this resulted in low-state and high-state PCA spectra which had smaller exposure times than the corresponding *Chandra* spectra. We obtained exposure times of 33.712 ks and 15.888 ks for the low-state and high-state PCA spectra respectively. Strictly speaking this does not sample the same time intervals as *Chandra* so we shall bear this in mind when interpreting the *RXTE* data. The implicit assumption is that those parts of the low and high states ‘missed’ by *RXTE* are, on average, spectrally similar to the parts that are not missed. The mean 3–15 keV background-subtracted count rates for the combined PCU0 and PCU2 spectra were 2.709 ± 0.011 ct/s and 3.971 ± 0.017 ct/s for the low-state and high-state respectively.

The time intervals derived from the *Chandra* intensity selection consist of alternating low and high states. The longest interval between those alternate states was 12.544 ks (not including the large $\sim 1/3$ day gap in the data – see Fig. 1). Thus, if we find variability in spectral features observed by *Chandra*, that variability would be occurring on a timescale of < 12.544 ks, since the mean count rate, lightcurves, and spectra are

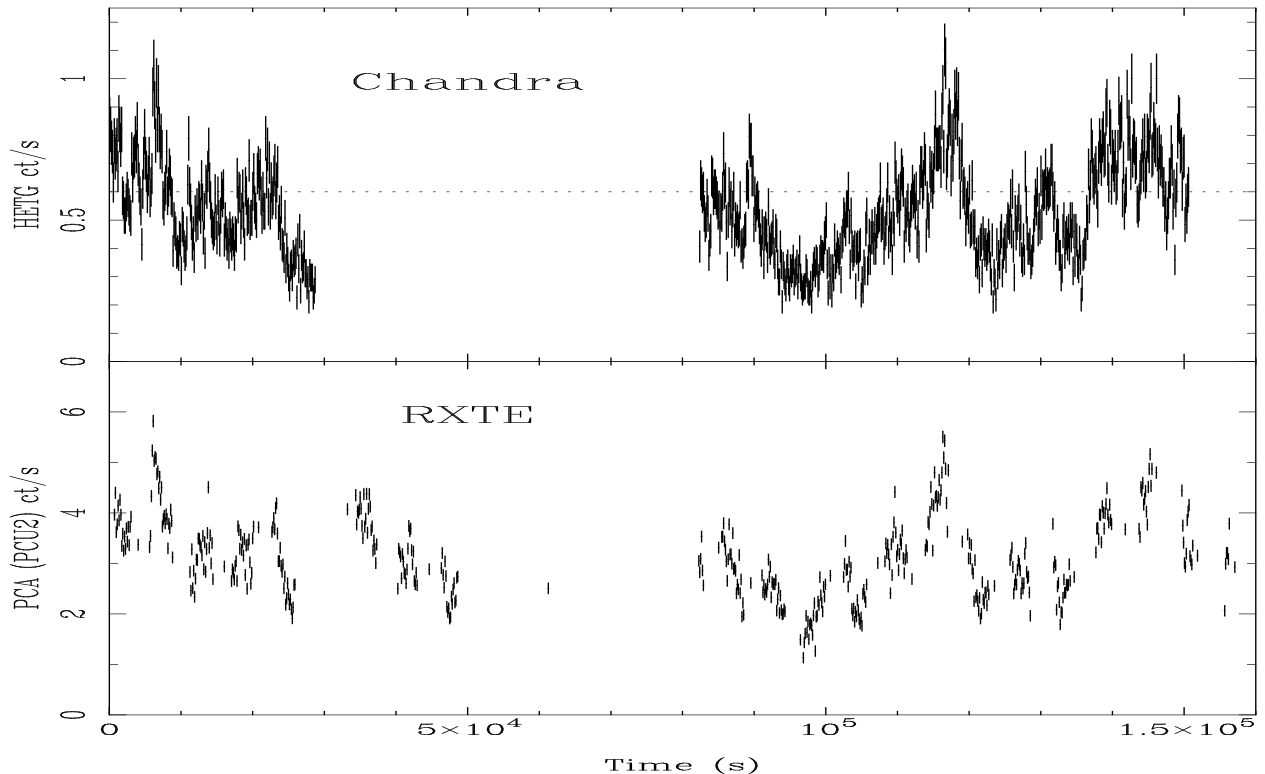


Figure 1. *Chandra* HETGS and *RXTE* PCA lightcurves of NGC 7314 binned at 128s. The HETGS data are from combined HEG and MEG ± 1 orders (0.8–7 keV). The PCA data are from PCU2 only (3–13 keV). The reference time corresponding to $t = 0$ for both lightcurves is 2002 July 19, UT 04:33:36.

similar either side of the gap. If the mass of the central black hole in NGC 7314 is $5\alpha \times 10^6 M_\odot$ (where $\alpha \sim 1$ – see §1) then 12.544 ks corresponds to a light-crossing distance of $\sim 502r_g/\alpha$ and a Keplerian orbital radius of $\sim 18.5\alpha^{-2/3} r_g$ (where $r_g \equiv GM/c^2$).

3. HIGH-RESOLUTION, TIME-RESOLVED SPECTROSCOPY

Below we describe spectral fitting of the mean, low-state and high-state spectra, using XSPEC v11.2 (Arnaud 1996). The C -statistic was used for minimization and, unless otherwise stated, all statistical errors correspond to 90% confidence for one interesting parameter ($\Delta C = 2.706$). All model parameters will be referred to the source frame using $z = 0.004760$, unless otherwise stated. As mentioned in §1, this value of redshift was obtained by Mathewson & Ford (1996) using

H I measurements so is probably the most accurate available. The range of measurements of z in NED⁴ correspond to an uncertainty of less than 10 km s^{-1} , which is much less than the systematic uncertainty in the HETGS wavelength scale ($\sim 433 \text{ km s}^{-1}$ ($\sim 11 \text{ eV}$) at 6.4 keV for the HEG⁵).

The MEG 0.5–5 keV mean spectrum can be described by an absorbed power law with photon index 1.99 ± 0.06 and column density $10.2^{+0.6}_{-0.5} \times 10^{21} \text{ cm}^{-2}$, plus $(4.3 \pm 0.5)\%$ of the direct, unabsorbed component of the power-law continuum. Similar spectral fitting of the low-state and high-state spectra reveal no evidence of variability in the column density, power-law slope, or scattering fraction. However, the power-law slope is not well-constrained and we will show below (§5) that

⁴NASA Extragalactic Database

⁵<http://space.mit.edu/CXC/calib/hetgcal.html>

the *RXTE* data do show variability in the slope. Hereafter, for *Chandra*, we will discuss only the HEG spectra since we are primarily interested in the Fe-K region, and the energy resolution and effective area are superior to the MEG at high energies.

3.1. Rapid Variability of the Fe-K Complex

Fig. 2 (a) shows the low-state HEG spectrum in the 5.5–8.5 keV observed energy range. Fig. 2 (b) and Fig. 2 (c) show the HEG high-state and mean spectra, respectively. Dotted lines show the expected positions of the Fe I $K\alpha$ line, the Fe XXV He-like triplet, and the Fe XXVI Ly α and Ly β lines. In the low-state spectrum shown in Fig. 2 (a) there are actually five discrete emission-line features immediately apparent in the 5.5–8.5 keV band. One is at an energy consistent with Fe I $K\alpha$ at 6.400 keV in the source frame, although the energies of $K\alpha$ lines from all ions up to Fe XVII differ from 6.400 keV by less than the *Chandra* HEG resolution (FWHM ~ 39 eV). Hereafter, we shall refer to this line as Fe $K\alpha$ (I). Another emission line in Fig. 2 (a) is near the expected energy for the He-like forbidden line but redshifted, and a third is near that expected for Fe XXVI Ly α , again redshifted. Although this redshift is small (~ 35 eV), it is significant. The systematic uncertainty in the energy scale is a factor of ~ 3 less than the redshift of the Fe XXV and Fe XXVI $K\alpha$ lines. The Fe $K\alpha$ (I) line is not redshifted relative to 6.400 keV. However we do not know the dominant ionization stage of Fe producing the Fe $K\alpha$ (I) line, so a redshift consistent with the Fe XXV and Fe XXVI $K\alpha$ lines is not ruled out.

Fig. 3 shows two-parameter joint confidence contours for intensity of line emission versus energy for the low-state, mean, and high-state spectra in the 6.1–7.1 keV band. The confidence levels correspond to 68% (blue), 90% (red), and 99% (black). The contours were generated by fitting a simple power-law continuum in the 5–9 keV band (see below for details) and constructing a grid of ΔC values when a narrow ($\sigma = 1$ eV) Gaussian component is added to the model, whose energy and intensity were traced over the range 6.1–7.1 keV and $0\text{--}6 \times 10^{-5}$ photons $\text{cm}^{-2} \text{s}^{-1}$ respectively. Here, and in subsequent spectral fitting, the low-state and high-state spectra were binned at 0.01\AA and the mean spectrum was binned at 0.005\AA (the HEG FWHM resolution is 0.012\AA).

In the low state there are three clear and isolated, discrete emission features in the 6.1–7.1 keV band, corresponding to $K\alpha$ emission from Fe I–Fe XVII, Fe XXV, and Fe XXVI. Fig. 2 and Fig. 3 clearly show that the complex of Fe-K emission, and therefore the ionization balance of Fe, is rapidly variable on timescales < 12.5 ks. It appears that as the continuum level increases (by a factor of ~ 1.7 from low-state to high-state), the ionization structure of the emitting region changes to produce a complex and variable blend of emission, instead of three, simple, discrete emission lines. Note that the signal-to-noise of the low-state and high-state spectra is approximately the same, and the signal-to-noise of the mean spectrum is approximately twice that of either low-state or high-state spectra alone. Therefore the differences between the contours in different states (Fig. 3) are *not* due to signal-to-noise effects. Nor are the differences simply the result of line emission becoming less significant against a rising continuum. Fig. 3 shows that the *centroids and widths* of the line emission near 6.4 keV and 6.6 keV appears to vary. It also appears that the Fe XXVI Ly α emission becomes broader. Detailed spectral fitting (described below) shows marginal evidence that the Fe XXVI Ly α centroid energy is higher by ~ 10 eV in the mean spectrum relative to the low-state. The intensity of Fe XXVI Ly α appears to be consistent with a constant in all three spectra (see Fig. 2, Fig. 3, and Table 1). However, the behavior of the intensity of this line in response to continuum variations is not expected to be simple because as the continuum level increases, more Fe XXV may get ionized to Fe XXVI, but at the same time more Fe would become completely stripped. Below we examine the low-state, mean, and high-state spectra in more detail.

3.2. Detailed HEG Spectra Around the Fe-K Complex

Fig. 2 (a) shows that there is a tentative detection of Fe XXVI Ly β which has a redshift that is consistent with Fe XXVI Ly α (details in §3.2.3). There is also a strong emission line which is unidentified (it is at ~ 5.84 keV in the source frame). There are no candidate atomic features near 5.84 keV which have high enough oscillator strength and elemental abundance to produce the line, and yet do not also predict other features which should be stronger but are not ob-

served. We can certainly eliminate any instrumental artifact being responsible because the line is almost undetected in the high-state spectrum (Fig. 2 [b]) and weak in the mean spectrum (Fig. 2 [c]). It is also not a background feature: the background spectrum, extracted from 3.6–10 arcsec either side of the dispersion axis is shown plotted in green in Fig. 2 (a). The most likely origin of the ~ 5.84 keV feature is Fe $K\alpha$ emission which has suffered gravitational and Doppler energy shifts in a spatially localized region near the central black hole, and this is discussed in detail in §4.2.

Initially, we fitted the four strongest emission lines (i.e. all except the Fe xxvi Ly β line) in the low-state spectrum, with Gaussians. By fitting the continuum in two different ways, we demonstrate, for the low-state spectrum, that the derived line parameters are robust to different assumptions about how the continuum is modeled since the lines are clearly narrow compared to the spectral resolution. In the first method we simply fitted a power law in the 5–9 keV range (as well as the four Gaussians). We found that extrapolation of this power law back down to 3 keV still provided an excellent description of the data. In the second method, we fitted the 0.8–9 keV data with an absorbed power law (omitting the 2–2.5 keV band due to systematic residuals around sharp changes in the effective area of the telescope – see Yaqoob *et al.* 2003), plus the four Gaussians. We then used the best-fitting photon index and ignored the data below 5 keV. In both cases the photon index was frozen to obtain the statistical errors on the Gaussian parameters. The intrinsic widths of the Gaussians were fixed at 1 eV (i.e. much less than the spectral resolution), but we allowed them to float one at a time in order to obtain upper limits. All four emission lines are unresolved by the HEG. Full results are shown in Table 1. It can be seen from Table 1 that the line parameters for the two continuum forms used are either identical or indistinguishable. Therefore we simply used the first method (simple power law fitted over 5–9 keV) for modeling the continuum for the mean and high-state spectra. Full results of the continuum plus line fits to the mean and high-state spectra are shown in Table 1. Note that the best-fitting model to the low-state spectrum (first method) is shown as a red solid line in *all* the panels of Fig. 2.

We estimated the significance of each of the

four detected emission lines in the low state by removing each emission line from the best-fitting four-Gaussian model and then re-fitting the model, noting the increase in the C -statistic. The best-fitting four-Gaussian model was then replaced before investigating another line in the same manner. The 5.842 keV line was detected only with $\sim 99\%$ confidence, and its equivalent width (EW) is 32^{+64}_{-16} eV. The Fe $K\alpha$ (I) line was detected with a confidence level $> 4\sigma$, and the $K\alpha$ lines from Fe xxv, and Fe xxvi were detected at $> 3\sigma$ confidence. The EWs of Fe $K\alpha$ (I), Fe xxv (f), and Fe xxvi Ly α in the low-state spectra are 81^{+34}_{-34} , 59^{+25}_{-34} , and 68^{+53}_{-30} eV respectively (see Table 1). The $K\beta$ line corresponding to the Fe $K\alpha$ (I) line is not detected, but by adding another narrow Gaussian at 7.058 keV (source frame) to the best-fitting, four-Gaussian, low-state model, we obtained upper limits on the intensity and EW of the Fe $K\beta$ line of 1.6×10^{-5} photons $\text{cm}^{-2} \text{s}^{-1}$, and 62 eV respectively, using the low-state spectrum. This is consistent with the Fe I $K\beta:K\alpha$ branching ratio of 17:150 (e.g. Bambynek 1972).

Fig. 2 (b) and Fig. 3 show that in the high state the line at 6.4 keV is hardly detected, but a new emission feature appears at ~ 6.3 keV. However, it is detected only at $\sim 96\%$ confidence. Nevertheless, for completeness, we model it with an additional Gaussian component and include the results in Table 1 and refer to the feature as Fe $K\alpha$ (II).

3.2.1. The Fe xxv He-like Triplet

The Fe xxv He-like triplet is potentially a powerful diagnostic of density and temperature. However, we note that the separation of the forbidden and intercombination lines and the intercombination and resonance lines is only 31.2 and 14.5 eV respectively⁶, less than the HEG FWHM (43 eV) at the observed energy of the intercombination line. We *assume* that the observed Fe xxv line is principally the forbidden line, since the measured redshift of 1350^{+780}_{-510} km s^{-1} (relative to the systemic velocity of NGC 7314) is then consistent with the redshift of 1500^{+480}_{-780} km s^{-1} for Fe xxvi Ly α (see Table 1). For Fe xxvi Ly α we used a rest energy of 6.966 keV: a branching ratio

⁶We take the energies of the forbidden (f), intercombination (i), and resonance lines (r) from NIST (<http://physics.nist.gov/PhysRefData/>): 6.6365, 6.6677, and 6.6822 keV respectively.

of 2:1 for the $\text{Ly}\alpha_1$ ($\lambda 1.778$) and $\text{Ly}\alpha_2$ ($\lambda 1.783$) components gives a centroid energy of 6.966 keV (Pike *et al.* 1996).

If the Fe XXV line were the intercombination or resonance line, the redshifts would be 2730 km s^{-1} and 3380 km s^{-1} respectively. However, we note that the upper limit on the width of the Fe XXV line (low state) is about twice that of Fe XXVI $\text{Ly}\alpha$, although they have similar EW (see Table 1). Until *Astro-E2* resolves the He-like Fe triplet, we will assume it is dominated by the forbidden line. For the forbidden line to dominate, the electron density should be less than $\sim 10^{16} \text{ cm}^{-3}$ (e.g. Bautista & Kallman 2000).

We obtained upper limits on the intensities of the intercombination (i) and resonance (r) lines of 0.6 and $0.7 \times 10^{-5} \text{ photons cm}^{-2} \text{ s}^{-1}$ respectively, by adding narrow Gaussians, one at a time, at energies redshifted from systemic by the same redshift as Fe XXVI $\text{Ly}\alpha$. Then, taking the lowest intensity in the measured range (low state) of what we assume is the forbidden line, we obtained lower limits on $R \equiv f/i$ and $G \equiv (f+i)/r$ of 1.3 and 1.1 respectively. As Bautista & Kallman (2000) point out, caution should be exercised with the use of R and G as density and temperature diagnostics respectively, since they are sensitive to whether the plasma is collisionally ionized or photoionized. Also, there are many dielectronic satellite features from He-like Fe in the range 6.61–6.71 keV (Oelgoetz & Pradhan 2001). Nevertheless, the density curves in Bautista & Kallman (2000) are consistent with $n_e < 10^{16} \text{ cm}^{-3}$ and the temperature curves indicate that $T < 10^{6.6} \text{ K}$ or $T < 10^{7.6} \text{ K}$ for collisional and photoionized gas respectively. Note that even the higher temperature corresponds to a thermal Doppler width of only $\sim 100 \text{ km s}^{-1}$, much less than the HEG resolution, but is $\sim 37\%$ of the 6 eV FWHM resolution of the *Astro-E2* calorimeter at 6.7 keV.

3.2.2. Fe $K\alpha$ Line Emission from Distant Matter?

For the Fe $K\alpha$ (I) line, the velocities shown in Table 1 assume an origin in Fe I, for which the branching ratio of 2:1 for the $K\alpha_1$ ($\lambda 1.936$) and $K\alpha_2$ ($\lambda 1.940$) components gives a centroid energy of 6.400 keV (Bambynek *et al.* 1972). Ionization states up to Fe XVII will give a $K\alpha$ line centered at an energy which differs from 6.400 keV by less than the HEG resolution (FWHM $\sim 39 \text{ eV}$ at 6.4 keV). It can be seen (Table 1) that the Fe $K\alpha$

(I) line energy shift is consistent with zero, but obviously there is some uncertainty as to the dominant ions responsible for the emission.

Given the tentative rapid variability of the line emission near 6.4 keV, it is not clear whether there is a contribution to the line emission at 6.4 keV from distant matter. If the low-state Fe $K\alpha$ (I) line were predominantly from distant matter, one could estimate a lower limit to the distance of the emitter from an upper limit on the width of the line emission. Assuming a virial relation and an r.m.s. velocity of $\sqrt{3}V_{\text{FWHM}}/2$ (e.g. Netzer 1990), and using our measured upper limit of FWHM $< 3520 \text{ km s}^{-1}$ (Table 1), gives a location in the outer BLR or beyond, at $> 2.8\alpha$ light days from the central mass ($5\alpha \times 10^6 M_{\odot}$).

The amount of Fe in the line-of-sight is not sufficient to produce the observed EW of the Fe $K\alpha$ (I) line ($81 \pm 34 \text{ eV}$) and this further argues for the Fe $K\alpha$ (I) line originating close to the X-ray source, possibly in the accretion disk. The Fe-K edge optical depth ($\tau_{\text{Fe}} = 0.018$) inferred from the soft X-ray cut-off (neutral Hydrogen column density of 10^{22} cm^{-2} – see §3) can at most produce an EW of 8.5 eV, even if it fully covered the sky (e.g. see Krolik & Kallman 1987; Yaqoob *et al.* 2001). On the other hand, the upper limit on the threshold optical depth of an Fe I K-edge, obtained from directly fitting the HEG data with an edge model at 7.11 keV (rest-frame), is $\tau_{\text{Fe}} = 0.12_{-0.12}^{+0.14}$.

3.2.3. Diagnostics from the Fe $\text{Ly}\beta$: $\text{Ly}\alpha$ Ratio.

If Fe XXVI $\text{Ly}\alpha$ is observed then Fe XXVI $\text{Ly}\beta$ emission is *expected*, with a predictable relative intensity (which may be zero), from basic physics. The theoretical value of the Fe $\text{Ly}\beta$: $\text{Ly}\alpha$ ratio depends on the excitation mechanism for the Fe XXVI $\text{Ly}\alpha$ line (e.g. see Bautista *et al.* 1998; Bautista & Titarchuk 1999). Fe XXVI $\text{Ly}\alpha$ emission directly following recombination will be accompanied by an edge at 9.19 keV and no $\text{Ly}\beta$ emission. The $\text{Ly}\beta$: $\text{Ly}\alpha$ ratio for collisional excitation depends on temperature and is potentially a powerful temperature diagnostic. At low temperatures, the $\text{Ly}\beta$: $\text{Ly}\alpha$ ratio can be negligible, but it can be as high as 0.44 for $kT > 1 \text{ keV}$. In the case of resonant fluorescent excitation the $\text{Ly}\beta$: $\text{Ly}\alpha$ ratio depends on the intensity and shape of the radiation field and may be as high as 0.26. It should therefore be clear that measurement of,

or placing constraints on, the Fe Ly β :Ly α ratio is critically important even if Fe xxvi Ly β is not detected. This is especially true since some parts of parameter space predict Ly β :Ly α \sim 0.

Although the detection of Fe xxvi Ly β in our data is only marginal (at best, for the low-state spectrum, $\Delta C = 4.5$ for the addition of a Gaussian with two free parameters), we can measure the center energy and intensity. We obtain $E = 8.18_{-0.04}^{+0.03}$ keV, an intensity of $1.0_{-0.9}^{+2.7} \times 10^{-5}$ photons cm $^{-2}$ s $^{-1}$, and an EW of 59_{-53}^{+159} eV (all are source-frame quantities, measured from the low-state spectrum). The redshift relative to the expected energy of 8.250 keV ⁷ is $8.5_{-3.7}^{+4.6} \times 10^{-2}$, consistent with the redshift we measure for Fe xxvi Ly α of $5.2_{-1.5}^{+1.4} \times 10^{-2}$. Our absolute lower limit on the ratio of Fe xxvi Ly β to Ly α intensities is 0.05. Our measurement errors on the Ly β :Ly α ratio are obviously too large for this to be a useful diagnostic yet, but it is something future missions will very soon begin to address, yielding critical information from a simple measurement.

3.2.4. Absorption Lines in the High-State Spectrum

Fig. 2 (b) shows that the high-state spectrum has two narrow absorption features that are not present in the low-state and mean spectra. Using an inverted Gaussian added to the best-fitting high-state model (Table 1) we measure rest-frame energies of $6.000_{-0.034}^{+0.012}$ keV and $6.760_{-0.011}^{+0.018}$ keV, and corresponding equivalent widths of $16.5_{-7.7}^{+3.3}$ eV and $16.6_{-8.9}^{+4.4}$ eV respectively. The origin of neither is clear, since the energies do not correspond to any known atomic transitions which predict the appropriate absorption, without predicting other features which are not observed. If the features are due to Fe xxv resonance absorption, the lower energy line implies an inflow of $\sim 0.10c$, whilst the higher energy feature implies an outflow of $\sim 0.012c$. Although the statistical significance of either of the features is not high (99% and 97% confidence for the lower and higher energy line respectively), the physical implications are important enough to warrant attempting confirmation with future missions (especially for the lower energy line since evidence

for inflow is so rare). Moreover, unambiguous narrow Fe-K absorption features indicating velocities as high as $\sim 0.1c$ have been found by *XMM-Newton* in the NLS1 PG 1211 + 143 (Pounds *et al.* 2003).

4. PHYSICAL CONSTRAINTS FROM THE CHANDRA DATA

4.1. Geometry

While the redshifts of the Fe xxv (f), and Fe xxvi Ly β lines are tentative, the redshift of Fe xxvi Ly α is firm, and is a robust measurement. Since Fe xxvi Ly α is not resolved by the HEG, the upper limit on its width (Table 1) is also a robust, model-independent measurement. The redshift and width constraints on the Fe xxvi Ly α line cannot both be simultaneously satisfied if the line were produced in a fully covering spherical geometry. For spherical inflow or outflow one would expect a P Cygni line profile which is not observed. We quantified the possibility of a P Cygni line profile in the low-state data (where the lines are the clearest), by adding an inverted Gaussian to the continuum plus four-Gaussian line model (see §3.2). The inverted Gaussian (absorption line) was blueshifted from 6.966 keV by the same amount as the observed Fe xxvi Ly α line is redshifted from 6.966 keV. We obtained a best-fitting equivalent width of zero and a one-parameter, 90% upper limit of 14 eV. This is to be compared with the measured EW of 68_{-30}^{+53} eV for the Fe xxvi Ly α emission line (Table 1). If the He-like line is the forbidden or intercombination component, it could not of course have a P Cygni line profile. If the He-like line is the red part of a P Cygni line profile from the resonance transition, the emission should extend all the way to the rest energy but it clearly does not (Fig. 2 and Fig. 3). We conclude that the data do not support a P Cygni line profile for the He-like and H-like lines.

In the case of Keplerian orbits in a spherical distribution, if the line-emitting matter were close enough to produce the required redshift and satisfy the time-variability constraints, the line profile would become broader than observed. A partially covering (or partially obscured) spherical geometry or cone model (e.g. see Zheng, Sulentic, & Binette 1990; Sulentic *et al.* 1998), or anisotropic illumination model (Yaqoob *et al.* 1993) would involve very restricted solid angles

⁷We take the wavelengths of 1.5024Å and 1.5035Å for Fe xxvi Ly β_1 and Ly β_2 respectively, from Verner, Verner, & Ferland (1996). The branching ratio of 2:1 for Ly β_1 :Ly β_2 gives a centroid energy of 8.250 keV

(to satisfy the constraint that the lines are not resolved by *Chandra*). Moreover, the structure or illuminating cone must be one-sided to give only a redshift and not a blueshift as well. To be sure, a bi-polar inflow or outflow, or wind, in which the approaching side is obscured, cannot be ruled out. For example, if the flow were aligned with the rotation axis of an accretion disk, and the linear extent of the flow were smaller than the disk radius, and if the system were viewed close to face-on with the flow facing away, then the approaching side of the flow would be hidden from view. However, the solid angle subtended at the continuum X-ray source by such a flow would be too small to produce the fairly large EW of Fe XXVI Ly α (~ 70 eV in the low-state spectrum and ~ 60 eV in the mean spectrum). It is also difficult to explain the line redshift and width constraints in terms of the wind outflow model of Elvis (2000) without further fine-tuning of the model. To overcome the blueshift from the outflow (in order to give an observed redshift), the wind must be placed closer to the black hole in order for gravitational redshifts to compensate, but then the lines would be broader than observed.

It is conceivable that the the 5.842 keV and 6.931 keV lines could be from a highly collimated jet (bulk velocity, $> 0.055c$), seen nearly end-on, since these line are approximately equidistant from 6.4 keV? The small difference of 27 eV would then be due to a slight difference in the angles of the receding and approaching sides of the jet relative to the line of sight. This scenario is unlikely because the narrow line widths require a small dispersion in the bulk velocity of $\sim 10\%$ and the scenario does not account for the 6.607 keV line.

All of the above models must also account for the rapid response (< 12.5 ks) of the ionization balance of Fe to the X-ray continuum variability. Given the amount of fine-tuning and/or incompatibility with the data, we consider the most viable and least-contrived origin of the line emission from highly ionized Fe to be the accretion disk itself.

4.2. The Origin of Narrow Lines from Disks

If the unresolved narrow emission lines observed by *HETGS* are from a disk there are three possible reasons for them to be narrow, which we summarize below.

(1) The lines could be from individual ‘hot

spots’ on the disk, whose orbital period is less than the length of the observation. The line width is then determined by the arc length traveled by the rotating hot spot during the observed time, and by the spread in radial coordinate.

(2) A given observed line could be the red or blue Doppler horn of a much wider line profile, originating in a ring of emission from either a single hot spot observed for more than one orbit, or a collection of hot spots observed for less than one orbit that are distributed in the form of a ring. The ring cannot have too large of a spread in radius because emission from different radii will effectively broaden the red and blue horns and therefore the observed line. MHD simulations by Armitage and Reynolds (2003) show that hot spots can survive for several orbits and are capable of producing sharp ‘spikes’ such as those observed here.

(3) The *entire* line profile may be from a large area on the disk but it may still so narrow that it is unresolved even by *Chandra*. This could happen for disks which have a flat radial line emissivity and are near face-on. In this case, we are no longer restricted to hot spots or annuli of emission since the red and blue Doppler horns are not resolved, so the emission could even extend down to small radii, if the radial emissivity law is flatter than r^{-2} .

In the case of (1) and (2), for a given disk inclination angle, there is only a very restricted choice in the radial coordinate (r/r_g) in order to match the observed line energies with the predicted energies. Therefore, it would have to be a remarkable coincidence for the observed energies of 6.607 keV and 6.931 keV (Table 1) to lie so close (within only ~ 1500 km s $^{-1}$) to the rest energies of Fe XXV (f) and Fe XXVI Ly α respectively. The extent of the fine tuning required by scenarios (1) and (2) is illustrated in Fig. 4, which shows the relation between the disk inclination angle, θ (for the extreme envelopes $\theta = 0^\circ$ and $\theta = 90^\circ$), and the radial coordinate, for a given rest energy of the line. Blue and red curves indicate emission from approaching and receding sides of the disk. Horizontal lines in the panels on the left are shown for line rest energies of $E_0 = 6.400, 6.636,$ and 6.966 keV. Each pair of panels in Fig. 4 corresponds to the energy of an observed line (6.931, 6.607, and 5.842 keV, as indicated). A solution exists where lines of a given E_0 would intersect blue and red curves of a given θ . This gives r/r_g

and also indicates that the energy range of the whole line profile covers the vertical interval in E_{obs}/E_0 at that r/r_g , which is contained inside blue and red curves corresponding to the correct disk inclination angle. This inclination angle cannot be determined uniquely without measuring both red and blue Doppler horns, as the right-hand panels of Fig. 4 show (although the plots also show that there are some restrictions on θ). Note that we would not necessarily be able to observe both red and blue horns in scenarios (1) and (2) even in principle, since the line emission may be distributed axis-symmetrically. Moreover, if $E_{\text{obs}} < E_0$ then the observed line may be *either* the red horn *or* blue horn of the full line profile (but if $E_{\text{obs}} > E_0$ the observed line is *always* the blue horn since gravitational and transverse energy shifts can take a blue horn below E_0 but can never take a red horn above E_0).

In scenarios (1) and (2) above, the only way to avoid fine tuning is to have r/r_g large enough and θ small enough that the observed center energy of a particular line energy is never very far away in energy from the rest value. However, in this part of parameter space, scenarios (1) and (2) go smoothly to scenario (3) anyway, in which the red and blue horns are so close in energy to each other that they are not resolved. This also requires that the 6.607 keV and 6.931 keV lines must indeed be associated with Fe XXV and Fe XXVI (see Fig. 4). Also, in the regime of large radius and small inclination angle, scenarios (1) and (2) require that the Fe XXV and Fe XXVI $K\alpha$ lines must originate from the receding side of the disk only in order to produce the observed redshifts.

Thus, since scenarios (1) and (2) require such highly contrived circumstances and fine-tuning, scenario (3) is the most likely to be applicable to the He-like and H-like Fe $K\alpha$ lines in the NGC 7314 data. In that case, no fine-tuning is required, and in particular, the line emission does not have to be concentrated in a narrow range of radii, nor is there any special requirement about the azimuthal distribution of line emission from the disk. In any case, our conclusion is testable with a second *Chandra* observation: the center energies of the 6.607 keV and 6.931 keV (low-state) lines should be significantly different next time if scenarios (1) or (2) above are applicable. This is because scenario (1), a hot spot origin, requires special values of radius *and* azimuthal angle of the hot spot on the disk, whilst scenario

(2), emission from an annulus, requires a special radius. It is of course highly improbable that we would observe a hot spot at the same radius, let alone at the same azimuthal angle as well. Therefore, in a second observation, if there were no measurable difference in the line energies relative to the first observation, and if scenario (2) applies, one would have to conclude that there is a special radius and that we are again observing only the red Doppler horn of a line profile originating in the same (receding) half of the disk as in the first observation. A far more plausible interpretation of immeasurable differences in the line energies from observation to observation would be that the red and blue Doppler horns are not resolved, as in scenario (3) above. Not too far in the future, *Astro-E2* will measure the narrow line profiles directly with a factor ~ 6.5 better spectral resolution and settle the issue. Until we obtain evidence to the contrary, we will assume scenario (3) for the He-like and H-like Fe $K\alpha$ lines in NGC 7314.

4.2.1. Origin of the 5.842 keV Feature

The above arguments against a hot-spot or annulus origin of the 6.607 keV and 6.931 keV lines do not apply to the 5.842 keV feature because it is not close to the rest energy of any Fe $K\alpha$ line. However, it is easy to rule out a hot-spot origin for the 5.842 keV feature. The most significant detection of this line is from the low-state spectrum, which is made of time intervals covering a total time period of ~ 100 ks (the length of the observation). Therefore, by definition, a hot spot must have $r \gg 330r_g$, otherwise we would be integrating over more than orbit and we would have an annulus of emission, not a hot spot. However, in order to get sufficient gravitational and Doppler redshifting, Fig. 4(e) shows that we must have $r < 132r_g$ (this upper limit is for a rest energy of 6.400 keV; 6.966 keV gives an even smaller upper limit).

As mentioned in §4.1, the difference in energy between 6.400 keV and 5.842 keV is within 27 eV of the difference between 6.931 keV and 6.400 keV. Could the 5.842 keV and 6.931 keV lines correspond to the red and blue horns, respectively, of an Fe $K\alpha$ line from an annulus? We can solve the equations for gravitational and Doppler shifts (in a disk around a Schwarzschild black hole) for values of r/r_g and θ as a function of the line rest energy, E_0 . Solutions only exist

for values E_0 greater than 6.409 keV. For this rest energy, $\theta = 90^\circ$ and $r = 136r_g$. Since NGC 7314 is a type 1 AGN, smaller inclinations are more plausible and $E_0 = 6.966$ keV gives $\theta = 20.4^\circ$ and $r = 16.4r_g$. However, such an interpretation still requires fine tuning since θ and r have to be very special to give a Doppler blue horn so close to the rest energy of Fe XXVI Ly α . Moreover, since the ion fractions of Fe XXV and Fe XXVI are so intimately related, one would expect to observe a red horn corresponding to the 6.607 keV line; the latter in this scenario would have to be identified with the blue horn of a He-like Fe K α line. A red horn is predicted between 5.54–5.61 keV (depending on which He-like transition is applicable). However, a narrow Gaussian emission line fitted at 10 eV intervals in the 5.0–6.0 keV range gives a reduction in the fit statistic, ΔC , which is never greater than 4.

On the other hand, the 5.842 keV line could still originate in an annulus if the 6.931 keV line has nothing to do with the 5.842 keV line. The constraints are shown in Fig. 4 (e) and Fig. 4 (f). These figures show that for small enough radii (and correspondingly small inclination angles), the 5.842 keV line could actually be the *blue* Doppler horn of a wider line profile. The transition radius, between the line being a red or blue Doppler horn, is $17.1r_g$ for $E_0 = 6.400$ keV and $9.3r_g$ for $E_0 = 6.966$ keV. We cannot resolve the ambiguity in the parameters without more information.

4.2.2. Comparison with NGC 3516

Narrow lines attributed to localized Fe K α emission from an accretion disk were reported by Turner *et al.* (2002) in another Seyfert 1 galaxy, NGC 3516, at energies of $\sim 5.57 \pm 0.02$, 6.22 ± 0.04 , 6.53 ± 0.04 , 6.84 ± 0.01 , and 6.97 ± 0.06 keV (in addition to the main peak at 6.41 ± 0.01 keV). The 6.84 keV and 6.97 keV lines are close to the rest energy of Fe XXVI Ly α so the same arguments given in §4.2 with respect to the 6.931 keV and 6.607 keV lines in NGC 7314 apply (namely, that their origin in hot spots or annuli is unlikely). The remaining lines are likely to be due to enhanced emission at particular radii, as discussed in Turner *et al.* (2002).

There is no conflict between the results and interpretation of the narrow Fe K α emission lines in NGC 7314 and NGC 3516. Nor is there any conflict in the different interpretation of the width of

different lines in the same source. Line emission integrated over the surface of a disk which has a flat radial line emissivity and which is viewed at small inclination angles will naturally give rise to an emission line profile which is narrow and which peaks close to the rest energy of the line if the outer radius of emission is large (several hundred r_g). Enhanced emission from localized regions on the same disk will give narrow emission lines which could be hundreds of eV away from the line rest energy.

4.3. Relation Between Energy Shift and Width of Disk Lines

We argued in §4.2 above, that the most likely reason for the Fe XXV (f) and Fe XXVI Ly α lines in NGC 7314 to be narrow is that they originate in an accretion disk which is nearly face-on and which has a flat radial line emissivity. In that case the red and blue Doppler horns are unresolved by the *Chandra* gratings. For emission lines originating in a disk rotating around a central mass, if the Doppler horns are unresolved, there is a definite relation between the minimum width, W_{\min} , of a line and its shift in centroid energy, ΔE , for a given disk inclination angle and *maximum* emission radius. Note that the line emission may extend down to small radii but the *minimum width* corresponds to the separation of the extreme red and blue Doppler horns at the maximum radius. *Independent of the radial emissivity profile of the line*, the line width cannot be smaller than this. Recall that we have rejected a hot-spot or annulus origin of the lines. We calculate W_{\min} and ΔE in a very simple-minded way as follows. We assume a Keplerian disk rotating around a Schwarzschild black hole, and calculate, for a given disk inclination angle, and line emission from a ring at a given r/r_g ($r_g \equiv GM/c^2$), the smallest and largest energy shifts measured by a distant observer (also taking into account gravitational redshifting). The minimum width as a function of r/r_g is then taken simply as the difference between the two extreme energies (i.e. the separation of the red and blue Doppler horns), and the energy shift is simply calculated as the average of these two extreme energies. The true centroid energy should take account of the differences in intensities of the red and blue horns due to relativistic effects. However, we cannot currently measure the shape of the lines in question so the approximation is adequate for our purpose.

Note that our assumption of a monochromatic line makes W_{\min} an even firmer lower limit on the width. For example, the Fe I $K\alpha$ and Fe xxvi Ly α lines each consist of two lines, separated by ~ 13 eV, and ~ 19 eV respectively (the higher-energy component having twice the intensity of the lower-energy one).

If E_0 is the rest energy of an emission line we get, in the limit $r/r_g \gg 1$, $w \equiv (W_{\min}/E_0) \sim 2 \sin \theta \sqrt{(r_g/r)}$ and $\epsilon \equiv (\Delta E/E_0) \sim (r_g/r)(1.5 - \sin^2 \theta)$, where θ is the disk inclination angle. From these equations, one can eliminate r to obtain a relation between the minimum line width and the energy shift for a given disk inclination angle. It is clear that if any lines in the Fe-K region are unresolved by the *Chandra* HEG ($w < 0.005$), there is already a very severe constraint on the disk inclination angle (it has to be less than a few degrees), and the maximum emission radius ($r/r_g \gg 1$). Now if $\sin \theta \ll 1$ (disk near face-on), we get the simple result that $w \sim \epsilon^{1/2} \sqrt{(8/3)} \sin \theta$. Using this, and the low-state measurements of energy shift, and width upper limit on Fe xxvi Ly α (Table 1), gives the most conservative upper limit on the inclination angle. The best-fitting ϵ gives $\theta < 5^\circ$ and a maximum radius of $\sim 300r_g$. Using the lower limit on ϵ gives $\theta < 7^\circ$. Using the latter upper limit on θ then gives an upper limit on the maximum radius of $\sim 610r_g$.

The exact relation (i.e. not assuming $\sin \theta \ll 1$ or $r/r_g \gg 1$) between minimum line width and energy shift is shown in Fig. 5 for various inclination angles (1000 w is plotted against 1000 ϵ). The radius goes from $10^4 r_g$ to $6r_g$ for each curve, from left to right respectively. The width/shift curves in Fig. 5 have a very general and simple interpretation for line emission from a disk *integrated over arbitrary radii, regardless of the radial emissivity of the line emission*. That is, for a given disk, any integrated emission line must lie *above* the curve corresponding to the correct value of θ for that disk. The measurements for a particular line plotted on the diagram cannot lie below the curve corresponding to the correct θ because large energy shifts in the line centroid must be accompanied by correspondingly large minimum line widths (i.e. separation of the Doppler horns). Therefore if we observe a particular emission line and its measurement errors place it below a line of given θ , then *all* values of θ greater than that are ruled out. Thus, the diagram is a powerful diagnostic.

The width upper limit and energy shift measurements for the Fe xxvi Ly α line in the low-state spectrum of NGC 7314 are shown Fig. 5. It can be seen that Fe xxvi Ly α alone immediately rules out inclination angles $> 7^\circ$, consistent with the simple estimate above. The measured upper limit on the width of Fe xxvi Ly α is very firm (it is unresolved by *Chandra*), as is shift from its rest-energy, so this line provides the tightest limit on the inclination angle. We include Fe xxv (f) in Fig. 5 even though its identification is tentative. As it happens, this line does not violate the constraint $\theta < 7^\circ$, but it also does not improve upon it.

4.4. Timescales, Disk Ionization Structure, and Radial Line Emissivity

We have shown that the ionization balance of Fe in the accretion disk responds rapidly to the continuum, on timescales < 12.5 ks. In the low state, the spectrum is dominated by $K\alpha$ lines from Fe xxv, Fe xxvi, and a line at ~ 6.4 keV from Fe I–Fe xvii. As the continuum intensity increases the line emission becomes complex, with more ionization stages between Fe I and Fe xxv contributing to the emission. We cannot tell how much of the line emission at ~ 6.4 keV comes from distant matter (see §3.2.2). However, if most of it comes from the disk, then a multi-phase medium is implied since Fe xxv and Fe xxvi cannot co-exist with significant ionization fractions of Fe I or so. A two-phase medium is indeed predicted by ionized disk models, which produce a warm/hot skin above an underlying cooler region (e.g. Nayakshin and Kallman 2001). The relative thickness of the skin is dependent upon, among other things, the shape of the X-ray continuum and the ratio of X-ray to disk flux. We note that the radiative recombination timescale for Fe xxv is $\sim 10 (10^{10} \text{ cm}^{-3}/n_e) (T/10^6 \text{ K})^{0.73}$ seconds (Shull & van Steenberg 1982), which is less than our 12.5 ks sampling time if the electron density (n_e) is not too small, or the temperature (T) not too high. In any case the temperature must be less than $\sim 10^9 \text{ K}$ since the Fe xxvi Ly α line is not resolved by the HEG.

Thus, it appears that when the continuum luminosity increases, either cooler material (e.g. the underlying disk) heats up, or warm/hot material (e.g. the skin) cools down, in order to produce more emission from the lower to intermediate ionization states of Fe. To obtain the full

picture one must observe the X-ray continuum out to higher energies, especially if the spectral shape varies with luminosity. In fact, we show in §5 that the X-ray spectrum is steeper in the high state than in the low state so that what we call the high state may have a lower ratio of hard X-ray to soft disk luminosity than the low state, when the broadband spectrum is taken into consideration.

We note that the hydrostatic timescale is $\sim 4.5\alpha(r/20r_g)^{\frac{3}{2}}$ ks (e.g. see Nayakshin & Kazanas 2002). At $6r_g$, this is ~ 740 s. The X-ray continuum in NGC 7314 varies on a timescale of hundreds of seconds, so the physical structure of most of the disk never has time to adjust itself in response to the X-ray continuum variability. We showed in §4.2 that the Fe XXV (f) and Fe XXVI Ly α lines in NGC 7314 likely originate in extended region on the disk, rather than a hot spot or localized annulus.

We emphasize again that the Fe XXV (f) and Fe XXVI Ly α emission may extend down to a few gravitational radii and still result in narrow emission lines (unresolved by the *Chandra* HEG). This is possible if the line emissivity (intensity per unit area) emissivity falls off with radius less steeply than r^{-2} (and may even be approximately uniform over some range in radius). The X-ray continuum source is likely to be distributed over the whole disk, possibly in the form of coronal flares (e.g. Haardt & Maraschi 1991, 1993; Svensson & Zdziarski 1994; Merloni & Fabian 2001). The flat emissivity could result from, for example, a roughly constant number of coronal flares of roughly equal intensity per unit area. A uniform illumination of the disk means that the line profile will be dominated by emission from large radii because of the larger area at larger radii. Thus, the red wing of the line profile, expected from the effects of strong gravity at the smallest radii for steeper emissivity laws, will be very weak. A small disk inclination angle then ensures that the entire line profile remains narrow. This is illustrated in the inset in Fig. 5, which shows the line profile, assuming monochromatic Fe XXVI Ly α (in the disk rest frame), from a uniformly emitting disk inclined at 3° , with the emission extending from $6r_g$ to $400r_g$, calculated using the method of Fabian *et al.* (1989). These parameters are a set consistent with the data. The dotted lines show the measured upper limits on the FWHM of Fe XXVI Ly α (Table 1). It can be seen

that the red wing may be too small to detect even with higher spectral resolution.

Ionized disk models generally predict that the He-like Fe K α line should be much stronger than the Fe XXVI Ly α line (e.g. Ballantyne *et al.* 2001; Nayakshin & Kallman 2001). This is because the models do not include turbulence so Fe XXVI Ly α is suppressed by resonant scattering. The fact that we observe the He-like and H-like lines to have about the same EW ($\sim 60 - 70$ eV in the low state), immediately tells us that turbulence must be significant. Invoking a region of parameter space of the disk in which the warm skin is negligible does not solve the resonant scattering problem because the H-like line is made in the skin itself.

Finally, we can also argue that the Thomson depth (τ_T) of the disk corona is probably much less than unity, simply from that fact that Fe XXVI Ly α is unresolved. Compton scattering in a corona with non-negligible optical depth would broaden the line. If the line were so broad that we only detect the unscattered component, the original line would have to a factor e^{τ_T} stronger than the observed line. The observed EW is already close to the maximum that can be produced by ionized disk models, even when resonant scattering is suppressed. However, collisional excitation of Fe XXVI Ly α could produce a larger (unscattered) EW. We note that a very large EW of Fe XXVI Ly α can be produced by bulk-Comptonization models (Bautista & Titarchuk 1999), but these are optically-thin and the observed line would be very broad, which is not the case in NGC 7314.

5. RXTE SPECTRAL ANALYSIS

Here we present spectral analysis of the low-state and high-state *RXTE* PCA spectra (combining PCU0 and PCU2). The extraction of these spectra was described in §2. As explained in §2, we shall utilize the 3–15 keV data only. Fig. 6(a) shows the ratio of the high-state spectrum to the low-state spectrum (both spectra were background-subtracted first). The ratio of 3–15 keV count-rates in the high-state spectrum to the low-state spectrum is 1.47 and this value is shown as a dotted, horizontal line in Fig. 6(a). It is clear that the high-state spectrum is softer than the low-state one. It does not appear to be a simple change in slope of the continuum, however.

There is a bump between $\sim 9 - 12$ keV.

The spectral resolution of the PCA in the Fe-K band is a factor ~ 30 worse than the *Chandra* HEG so we take the best-fitting parameters of the Gaussian emission-line models fitted to the HEG low-state and high-state spectra, and use them for spectral fitting to the corresponding PCA spectra. All the line parameters, including the intensities, will be frozen at the values given in Table 1, after correcting for the difference in HEG and PCA normalizations (see §2.1). For the low-state spectrum, the model involves four Gaussian emission-line components (Fe K α (I), Fe xxv, Fe xxvi Ly α , and the 5.842 keV line). For the high-state spectrum, we include an additional line, namely the redshifted Fe K α (II) component (see §3.2, and Table 1). Table 2 shows, not surprisingly, that these line models, when added to a simple power-law continuum with floating photon index (Γ) and normalization, give a poor fit to both low-state and high-state PCA spectra.

Below, we compare the *RXTE* data to various models of the X-ray reflection continuum from the accretion disk. However, it should be remembered that the X-ray continuum in NGC 7314 varies on a timescale of hundreds of seconds, yet the hydrostatic timescale is $\sim 4.5\alpha(r/20r_g)^{\frac{3}{2}}$ ks (e.g. see Nayakshin & Kazanas 2002). At $6r_g$, this is 740 s. Thus, most of the disk will not be in hydrostatic equilibrium, whereas the models assume equilibrium has been achieved.

5.1. ‘Cold’ Reflection

To the above power law plus Gaussian-lines model, we added a continuum component due to Compton-reflection in ‘cold’, solar abundance, optically-thick matter (using the XSPEC model PEXRAV – see Magdziarz & Zdziarski 1995). We fixed the inclination angle at the smallest value allowed by the model (18°), guided by our findings from the *Chandra* spectra. The direct, power-law model continuum is exponentially cut-off with a roll-over fixed at 100 keV. Thus, there is only one extra free parameter relative to the simple power-law plus Gaussian-lines model described above, and that is the ‘amplitude’ of the reflected continuum, R , relative to that expected from a time-steady X-ray source illuminating a reflecting medium which subtends a solid angle 2π at the source. The model improves the fits but the high-state fit is still very poor (see Table 2). The problem is that the high-state fit leaves residu-

als in the 6–7 keV band, which, if modeled by additional Fe line emission would imply at least twice the intensity of total Fe line emission than observed by *Chandra*. Also, the high-state spectrum has an edge-like feature at ~ 8 keV which is not modeled by the cold reflection model. In fact if we add a simple edge model (two additional free parameters: the threshold energy, and optical depth at threshold), we obtain good fits for both the low-state and high-state spectra. The best-fitting parameters are given in Table 2. It can be seen that the high-state spectrum does not actually require any reflection continuum and could just as well be fitted with a power-law and an absorption edge.

5.2. Ionized Disk Reflection: PEXRIV

We attempted to fit a *cold* Compton-reflection model because the Fe K α (I) line (see Table 1) detected by *Chandra* could originate in an optically-thick obscuring torus (viewed near face-on). Table 2 shows that such a reflection component could be present in the low-state spectrum, and that if (as expected) it does not respond to rapid continuum variability, it is at least consistent with being present in the high-state spectrum. However, we do not take these results literally, and the complexity added by the absorption edges that seem to be required rather suggests that we should attempt to fit models of reflection from an ionized medium. In that case the reflection continuum is much more complicated, and in particular the Fe K edge can be deeper and higher in energy compared to reflection in neutral matter (e.g. see Ballantyne *et al.* 2001; Nayakshin, & Kallman 2001). Therefore we removed the edges from the above model and replaced PEXRAV with PEXRIV (the latter is an ionized reflection model due to Magdziarz & Zdziarski, 1995).

The model PEXRIV computes only continuum and no line emission so we retained the Gaussian emission lines, their parameters still fixed at the best-fitting *Chandra* values (corrected for the HEG/PCA cross-normalization difference – see §2.1). The results are shown in Table 2. The best-fitting models and ratios of data to model for the low-state and high-state spectra are shown in Fig. 6(b). Good fits are obtained, but the low-state data still have a marked deficit between $\sim 10 - 11$ keV relative to the model. Table 2 shows that R is consistent with being the same (~ 1) for both the low-state and the high-state spectra,

within the errors. The PEXRIV model has two additional free parameters compared to PEXRAV: the disk temperature (T), and ionization parameter (ξ). The remaining parameters are kept fixed at their values in the PEXRAV model. We found that the disk temperature is essentially unconstrained in the low state (no value in the allowed model range of 10^4 – 10^6 K is preferred), and that the ionization parameter is not bounded below (upper limit, 56 erg cm s^{-1}). On the other hand, for the high-state spectrum the disk temperature is bounded below (at 1.2×10^5 K) and $\xi = 27_{-15}^{+62} \text{ erg cm s}^{-1}$. These results can be interpreted in terms of a reflection continuum being dominated by matter which is more strongly ionized in the high state than in the low state.

5.3. Ionized Disk Reflection: XION

Next, we replaced the PEXRIV model with the XION model in XSPEC (see Nayakshin & Kallman 2001). XION calculates the reflected spectrum from an X-ray illuminated disk self-consistently, balancing the hydrostatic and thermal structure of the disk. The model does not allow R to be varied (it is effectively fixed at unity). The inclination angle and exponential cut-off energy of the direct power law were kept fixed at the previous values. The inner and outer disk radii were fixed at $6r_g$ and $600r_g$ respectively. The model allows three choices of geometry: a central point-source illuminating the disk (‘lamp-post’ model), a central sphere illuminating the disk, or coronal flares illuminating the disk. We found that the choice makes negligible difference to the best-fitting parameters and no difference to our conclusions, and we quote results for the coronal flare case. The model also includes relativistic smearing.

The two parameters that we allowed to float in the XION model were the X-ray to disk luminosity, L_x/L_{disk} , and the accretion rate, normalized to Eddington, $\dot{m}/\dot{m}_{\text{Edd}}$ (see Nayakshin & Kallman (2001) for details). Finally, the model calculates line emission in addition to the reflection continuum. However, this is problematic because the model (in common with other disk illumination models) predicts Fe XXVI line emission to be weaker than Fe XXV emission, which is not what is observed in our data for NGC 7314 (the He-like and H-like lines have about the same EW). The reason is that turbulence is not included, so Fe XXVI Ly α is suppressed by resonant scattering. Also, the model does not allow small

enough inclination angles to predict the detailed Fe line emission that we observe (the minimum inclination allowed is 18°). Therefore we fitted the PCA spectra omitting the 5.5–7.5 keV region. The main purpose of these fits is to investigate whether we can obtain better fits to the continuum than PEXRIV, which contains less ionization physics.

The results are shown in Table 2 and Fig. 6(c) (the latter showing the best-fitting models and data/model ratios for the low-state and high-state spectra). The fits are excellent and we can see that the problematic feature in the data at ~ 10 keV is now fitted by an Fe recombination edge (which is absent from the PEXRIV model). On the other hand, we also see that the line emission predicted by the model is different to that observed, with the $K\alpha$ emission from Fe XXV being much stronger than that from Fe XXVI. The ratio L_x/L_{disk} is not well-constrained by the data although the upper limits suggest that the high-state spectrum may have a value up to an order of magnitude higher than the low state. For $\dot{m}/\dot{m}_{\text{Edd}}$ there appear to be two solutions for the low state: either this ratio is in the range 0.02–0.15 or it is > 0.27 . For the high state, $\dot{m}/\dot{m}_{\text{Edd}} < 0.36$. Thus, better data and modeling are required. What we can say is that the photon index of the power-law continuum is flatter in the low state than in the high state and when one considers the broadband continuum, it may be this spectral variability which is driving the ionization state of the disk. What we call the high state (defined as such by the luminosity in the narrow 0.8–7 keV band) may in fact correspond to a smaller L_x/L_{disk} since the high-state spectrum is steeper than the low state.

6. THE STUDY OF BLACK-HOLE ACCRETION-DISK PHYSICS USING NARROW Fe $K\alpha$ LINES

One of the major goals of Fe $K\alpha$ line studies in AGN is to ultimately map the space-time near the event horizon of a black hole. It is anticipated that this will be a key area for *Constellation-X* to break ground. A ‘yardstick’ with which we can gauge the precision with which we can map the space-time near the event horizon is the precision with which we can measure the black-hole angular momentum, or spin (a). The problem is that we do not currently understand the relation between

the X-ray continuum and relativistic Fe $K\alpha$ line emission in AGN well enough to construct realistic reverberation models (e.g. Ballantyne & Ross 2002; Shih, Iwasawa, & Fabian 2002). It is widely recognized that we first need to understand the ionization structure of the accretion disk and *its* relation to the X-ray continuum. Thus, our *Chandra* results for NGC 7314 are important because this source has an X-ray continuum which has a dynamic range of rapid variability large enough to be useful. NGC 7314 exhibits ionization stages of Fe from \sim Fe I up to Fe XXVI, and the ionization structure of Fe responds to the rapid continuum variability. These properties have not been demonstrated for any other AGN. If we want to use reverberation techniques to probe the space-time near the event horizon of a black hole we need to understand the ionization physics from an observational point-of-view, in order to build a theoretical understanding. To achieve this, we had better study NGC 7314 further, and identify other suitable sources too. In addition to pursuing reverberation mapping, there is a parallel approach we can pursue, described below, which does not rely on any knowledge of the relation between the X-ray continuum and the line emission.

6.1. Alternative Technique for Measuring Black Hole Spin

Spectra with a FWHM resolution of ~ 6 eV, obtainable in the very near future with *Astro-E2*, will determine whether our interpretation of the Fe xxv and Fe xxvi narrow Fe $K\alpha$ lines in NGC 7314 (i.e. emission from a large area of a disk having a flat radial line emissivity) is correct or not, by directly measuring the line profile. Once verified, the direct observation of narrow Fe xxvi Ly α line emission from the accretion disk in NGC 7314 will represent a critical step toward the goal of making precision measurements of key parameters of an accretion disk/black-hole system using future, high-throughput, high spectral resolution instrumentation because some of the current limitations of Fe-K line studies (aside from the variability problem), may be overcome.

Now, the precision with which we can measure the physical parameters of the accretion disk/black-hole system from an Fe $K\alpha$ line profile (principally, the inclination angle, θ , the inner and outer radii of emission, and the black-hole spin) depends directly on how well we can measure the energies of the red and blue Doppler

peaks at the outermost radii of emission, and the minimum and maximum energies of the extrema of the entire profile (corresponding to the innermost radii of emission). The Doppler peaks corresponding to the outer radii become broader (as does the entire line profile) and more poorly defined as θ increases, and as the radial line emissivity becomes more and more weighted toward smaller radii. At some point these peaks become so broad that higher spectral resolution does not help in improving the precision with which they can be measured. When the lines are very broad (FWHM ~ 1 keV or so), the maximum energy of the blue wing is the easiest to measure, but the minimum energy (the lowest energy of the red wing) is extremely difficult to measure since it merges smoothly with the continuum. The extent of the red wing will always be ill-defined, no matter how good the spectral resolution is. In addition to these problems, if the Fe $K\alpha$ line is due to the lower ionization states of Fe, the uncertainty in the line rest energy will present an inherent limit on the precision of measurement of the disk and black hole parameters. It should also be obvious that Fe $K\alpha$ lines from the lower ionization states of Fe are subject to confusion with non-disk Fe $K\alpha$ line emission from distant matter, which is difficult to disentangle without variability information.

On the other hand, narrow Fe $K\alpha$ lines from low-inclination disks are affected significantly less by these problems. A flat radial line emissivity is preferable (allowing larger inclination angles to give narrow lines) but not essential. If we can identify an emission line with Fe xxvi Ly α (as we can in NGC 7314) then the uncertainty in rest energy is eliminated. It will still be difficult to measure the extent of the red wing, but in what follows we will not require this to be measured. All we have to do is measure the energies of the two Doppler peaks corresponding to the outer radius of emission (r_{\max}), and the maximum energy of the blue wing corresponding to the approaching side of the disk at the inner radius (r_{\min}). All three quantities will be clearly defined for a narrow line. Therefore we have three measurements and four unknowns (r_{\min} , r_{\max} , θ , and a). Although the innermost stable orbit in a Kerr metric is related to a , we cannot simply assume that the line emission extends all the way to the last stable orbit. However, we can say that r_{\min} must be greater than the last stable radius. The

Doppler peaks corresponding to r_{\max} have a negligible dependence on a if $r_{\max} > 10r_g$. Thus, we can solve for r_{\max} , and θ , and get an upper limit on a , or we can get a relation between r_{\min} and a .

Now, in addition to a narrow Fe K α disk line, suppose we can identify a pair of red and blue Doppler peaks due to enhanced emission at a localized radius from the black hole. This radius must be less than $\sim 10r_g$ in order to measure the spin, but whether this is the case or not will be determined as part of the technique (and the data rejected if this is not the case). Then, measurement of the energies of the red and blue Doppler peaks gives us two observables for only three unknowns (the emission radius, r , a , and the line rest energy), since we have already measured θ from the main line profile, as discussed above. If the original line was Fe XXVI Ly α we may be able to deduce its identity simply from the fact that for the given θ , the next lowest Fe K α rest energy (at least 284 eV lower, for the Fe XXV resonance line) may not be able to produce a blue peak at an energy as high as observed whilst still satisfying the r_{\min} versus a relation deduced from the main line profile. Then we can solve for r and a . If it is not possible to deduce the rest energy, we look for another pair of red and blue Doppler peaks due to local emission from a different radius. It could be at a completely different time, even from a different observation, since it is reasonable to expect that θ and a are not going to change. Then we will have four observables for four unknowns (two emission radii, a , and the rest energy) so we can solve uniquely for a . Obviously the line rest energy must be the same for both events. If it is not the same we will know because we will not be able to obtain a unique solution. In that case we look for further events until we do obtain a unique solution.

As already mentioned, localized Fe K α line emission has already been observed in at least three AGN now (MCG -6-30-15, Iwasawa *et al.* 1999; NGC 3516, Turner *et al.* 2002; NGC 7314, 5.842 keV feature reported in this paper). Although it has not always been possible to identify both red and blue peaks of an event, the leap in effective area of *Constellation-X* should show these features effortlessly. In fact it would be more surprising if these localized events were *not* observed. We expect them to be observed with abundance by *Constellation-X*. It has been shown

that, at least for *Constellation-X*, even very modest localized enhancements, of the order of only $\sim 10\%$ of the total line emission, will be easily measurable in exposure times less than one day, for the bright, well-known AGN (Yaqoob 2001). For particularly strong feature, we will be able to track the center energy as a function of time and measure the black-hole mass (e.g. Nayakshin & Kazanas 2001).

It is important to realize that *nowhere in the above scenario for measuring black-hole spin did we ever have to measure, parameterize or know anything about the radial line emissivity*, even for measurements made from the main line profile. All that is required is that the main line profile is *observed* to be narrow, and the central red and blue Doppler peaks have enough definition to measure their energies with a precision matching the capabilities of the calorimeters on *Astro-E2* or *Constellation-X*. The drop on the blue side of the line profile will automatically be sharp under the above conditions. Although nothing about the line radial emissivity needs to be known, if the line profile is *observed* to have the above characteristics, the implication is of course that the inclination angle is small and the line radial emissivity flat.

6.2. Observation of Fe XXVI Ly α in Other Sources

It will now be necessary to re-examine and possibly re-interpret low spectral resolution data for AGN in general, in the light of our findings. Certainly, the iron line variability which was found by *ASCA* to be very common (e.g. Weaver, Gelbord, & Yaqoob 2001), in particular the variable centroid energy, will be easier to interpret in terms of variable proportions of emission-line intensities from different ionization states. Other puzzling line variability results from *ASCA* (e.g. Reynolds & Nowak 2003 and references therein) need to be re-examined. Ionized disk models make specific predictions about the variability of the Fe K α lines from different ions of Fe and direct comparison with the data is much easier for the Fe XXV and Fe XXVI lines, especially if they are not too broad (e.g. Ballantyne & Ross 2002; Nayakshin & Kazanas 2002).

There have been several reports of He-like or H-like Fe K α lines at low spectral resolution, using *ASCA*, *BeppoSAX*, *XMM-Newton* and even *RXTE* (e.g. Nandra *et al.* 1996; Turner, George,

& Nandra 1998; Comastri *et al.* 1998; Yaqoob & Serlemitsos 2000; Pounds *et al.* 2001; Reeves *et al.* 2001; Weaver *et al.* 2001; Turner *et al.* 2001; Matt *et al.* 2001; Reeves 2002; Perola *et al.* 2002). Only in two of these cases has the Fe $K\alpha$ line been identified with Fe xxvi Ly α (PG 1116+215, Nandra *et al.* 1996; Ton S 180, Turner *et al.* 1998, Comastri *et al.* 1998). There is evidence for Fe xxvi Ly α emission in MCG -6-30-15 from *XMM-Newton* data (Fabian *et al.* 2002) but this could not be distinguished from Fe xxv resonance absorption. These low-resolution data are subject to ambiguities from line blending when the line emission is very broad. For example, although optically-thin bulk-Comptonization models have been invoked to explain the EW of the line in Ton S 180 (Bautista & Titarchuk 1999), blending of lines from other ionization states of Fe cannot be ruled out.

Fang *et al.* (2002) report an Fe xxvi Ly α line from the quasar H 1821 + 643 using the *Chandra* gratings, but it was detected with a significance of only 2.3σ . We examined *Chandra* HETGS data for all type 1 AGN which are currently public and find marginal evidence of Fe xxvi Ly α in a few sources, but none as clear as NGC 7314 (Yaqoob *et al.* 2003, in preparation). It is worth remembering that the HEG effective area in the Fe-K band is tiny ($\sim 15 \text{ cm}^2$ at Fe xxvi Ly α). With future missions, which will have larger collecting area and better spectral resolution (such as *Astro-E2*, *Constellation-X*), we should expect the Fe xxv $K\alpha$ and Fe xxvi Ly α emission lines to play an important role in studying the black hole and accretion disk in AGN. Even *Astro-E2* will be able to resolve all three components of the He-like Fe triplet (see §3.2.1) and measure the Fe xxvi Ly α to Fe xxvi Ly β ratio (see §3.2.3), thus improving considerably the constraints on the ionization structure and physical conditions in the accretion disk and corona.

7. SUMMARY

We observed the low-luminosity, narrow-line Seyfert 1 galaxy NGC 7314 with the *Chandra* HETGS (simultaneously with *RXTE*). The source exhibited large-amplitude variability of the X-ray continuum, by as much as a factor of ~ 4 in ~ 3 ks. This is consistent with historical X-ray observations and its relatively small central mass of $5\alpha \times 10^6 M_\odot$ (where $\alpha \sim 1$). The most

important aspect of our results is that they establish NGC 7314 as a key laboratory for future missions to study the ionization physics of accretion disks. This is because the ionization structure of Fe varies rapidly in response to the large-amplitude X-ray continuum variations, and we detect ionization states of Fe from Fe xvii or lower, up to Fe xxvi. If we want to eventually map the space-time near the event horizon of a black-hole using reverberation of Fe $K\alpha$ lines, understanding the ionization physics of the accretion disk is a pre-requisite.

Below we summarize our results for NGC 7314.

1. We detected redshifted, unresolved emission lines from Fe xxv (f), Fe xxvi Ly α . Although the Fe He-like triplet is not resolved by *Chandra*, if the emission is dominated by the forbidden line, a consistent redshift is obtained for both Fe xxv and Fe xxvi ($cz \sim 1500 \text{ km s}^{-1}$).

2. The least contrived geometry for the line-emitting region is that of a disk. Other geometries are incompatible with the observational constraints and/or require much fine tuning.

3. The most likely reason for the Fe $K\alpha$ lines being narrow, which requires the least fine tuning, is that the disk inclination angle is small and the radial line emissivity (intensity per unit area) is flatter than r^{-2} (§4.2). In that case the line width and redshift constraints measured from Fe xxvi Ly α alone imply that the line emission comes from within ~ 600 gravitational radii of the putative central black hole, and that the disk axis is inclined at $< 7^\circ$ to the observer. Our interpretation of the data is easily testable with further observations, even with current instrumentation.

4. The Fe $K\alpha$ line emission may extend all the way down to a few gravitational radii of the black hole and yet still give an overall line profile which is unresolved by *Chandra*, if the radial line emissivity is flat. A coronal X-ray source extending over the disk could achieve this. This has important implications for AGN in general. If a disk is viewed at inclination angles close to face-on, and the radial emissivity (intensity per unit area) of an Fe $K\alpha$ line falls off less steeply than r^{-2} , the resulting emission-line profile may not have a prominent red wing. The line may not even be broad, even if the line emission extends down to a few gravitational radii of the black hole. Conversely, one cannot rule out a disk origin of an Fe $K\alpha$ line simply because it is narrow, even if it is unresolved by the *Chandra* gratings. The find-

ing of a variable narrow Fe $K\alpha$ line in Mkn 841 (Petrucci *et al.* 2002) supports these conclusions.

We emphasize that some AGN (such as MCG –6-30-15) clearly do have a strong red wing on the Fe $K\alpha$ line and *do* require a steep radial line emissivity. Our results should be interpreted in the sense that we have now probably observed the extreme ends of a distribution, with objects like NGC 7314 at one end (Fe-K disk lines unresolved by *Chandra*), and objects like MCG –6-30-15 (Fe-K disk lines several keV wide) at the other end.

5. The fact that the Fe XXV and Fe XXVI $K\alpha$ lines have comparable equivalent widths implies that turbulence is significant in the emitting medium, otherwise Fe XXVI Ly α would be suppressed due to resonant scattering. Future missions will be able to reliably measure the Fe XXV Ly β :Ly α ratio and resolve the Fe He-like triplet, and thus discriminate between different types of accretion models.

6. The X-ray continuum varies on a timescale of hundreds of seconds, which is faster than the hydrostatic timescale even for the innermost regions of the accretion disk so most of the disk is never in hydrostatic equilibrium. In the context of a disk-corona model, the Fe XXVI Ly α line must be formed in the ionized disk, as the corona itself cannot produce the required equivalent width. The corona is likely to be Thomson-thin, otherwise the Fe XXVI Ly α line would be broadened by Compton scattering.

7. The ionization balance of Fe responds to continuum variations on timescales less than 12.5 ks (which corresponds to a light-travel distance of $\sim 500/\alpha$ gravitational radii for $M = 5\alpha \times 10^6 M_\odot$).

8. Simultaneous *RXTE* data show that the continuum becomes steeper as the continuum luminosity increases, so what we call the high state (defined in terms of the 0.8–7 keV luminosity) may in fact correspond to a smaller ratio of broadband X-ray to disk luminosity, accounting for emission from lower ionization states of Fe in the high state.

9. The Fe $K\alpha$ line at ~ 6.4 keV (unresolved, with equivalent width, 81 ± 34 eV) as a center energy consistent with the $K\alpha$ line from Fe I–Fe XVII. The offset velocity relative to the systemic velocity of NGC 7314 depends on which ionization stages dominate the line emission (and is consistent with zero for Fe I). It is not clear

whether this component at ~ 6.4 keV originates in the accretion disk, distant matter, or both, since there is some evidence of rapid variability. If all of this line originates in distant matter, the upper limit on the width places it in the outer BLR or beyond. For a central mass of $5\alpha \times 10^6 M_\odot$ ($\alpha \sim 1$), this corresponds to a lower limit on the distance of > 9700 gravitational radii, or $> 2.8\alpha$ light days from the X-ray source.

10. When the X-ray luminosity in the $\sim 3 - 10$ keV band is low, hardening of the X-ray continuum, above ~ 10 keV, due to Compton reflection, is greater than that in a high state. The low state is dominated by reflection from low-ionization, optically-thick matter, and the high state is dominated by reflection from more highly ionized matter. The former might be associated with distant-matter and so would not respond to variability in the direct continuum. The reflection from ionized matter is likely present all the time, but responds to continuum variability and dominates the spectrum in the high state. There is tentative evidence of an Fe XXVI recombination edge in the *RXTE* data.

11. We presented details of a method by which future high throughput, high spectral resolution instrumentation could measure black-hole spin, without any knowledge or understanding of the relation between X-ray continuum and Fe $K\alpha$ line emission (§6.1). Using this method, the greatest precision will be achieved when the line emission from the accretion disk is due to Fe XXVI Ly α and when it is narrow.

The authors thank Peter Serlemitsos, Richard Mushotzky, Sergei Nayakshin, Martin Elvis, and Barry McKernan for valuable discussions. Support for this work was provided by NASA through *Chandra* Award Number GO2-3133X issued by the Chandra X-ray Observatory Center, which is operated by the Smithsonian Astrophysical Observatory for and on behalf of the NASA under contract NAS8-39073. The authors also gratefully acknowledge support from NASA grants NCC-5447 (T.Y., U.P.), NAG5-10769 (T.Y.), and NAG5-7385 (T.J.T). This research made use of the HEASARC online data archive services, supported by NASA/GSFC. This research has made use of the NASA/IPAC Extragalactic Database (NED) which is operated by the Jet Propulsion Laboratory, California Institute of Technology, under contract with NASA. The authors are grateful to the *Chandra* and *RXTE* instrument

and operations teams for making these observations possible, and to an anonymous referee for helping to improve the paper.

REFERENCES

1. Armitage, P. J., & Reynolds, C. S. 2003, MNRAS, submitted, (astro-ph/0302271)
2. Arnaud, K. A. 1996, *Astronomical Data Analysis Software and Systems V*, eds. Jacoby, G., & Barnes, J., p. 17, ASP Conference Series, Vol. 101
3. Ballantyne, D., & Ross, R. R. 2002, MNRAS, 332, 777
4. Ballantyne, D., Ross, R. R., & Fabian, A. C. 2001, MNRAS, 327, 10
5. Bambynek, W., Crasemann, B., Fink, R. W., Freund, H.-U., Mark, H., Swift, C. D., Price, R. E., & Rao, P. V. 1972, *Rev. Mod. Phys.*, 44, 716
6. Bautista, M. A., & Kallman, T. R. 2000, ApJ, 544, 581
7. Bautista, M. A., Kallman, T. R., Angelini, L., Liedahl, D. A., & Smits, D. P. 1998, ApJ, 509, 848
8. Bautista, M. A., & Titarchuk, L. 1999, ApJ, 511, 105
9. Branduardi-Raymont, G., Blustin, A., Wu, K., Kaastra, J., Kahn, S. M., & Deluit, S. 2002, in *Proc. High Resolution X-ray Spectroscopy with XMM-Newton and Chandra*, ed. G. Branduardi-Raymont, published electronically, http://www.mssl.ucl.ac.uk/~gbr/rgs_workshop/papers/branduardi_g_2.ps
10. Comastri, A., *et al.* 1998, A&A, 331, 31
11. Dickey, J. M., & Lockman, F. J. 1990, ARA&A, 28, 215
12. Done, C., Madejski, G. M., & Życki, P. T. 2000, ApJ, 536, 213
13. Elvis, M. 2000, ApJ, 545, 63
14. Fabian, A. C., Iwasawa, K.; Reynolds, C. S., & Young, A. J. 2000, PASP, 112, 1145
15. Fabian, A. C., *et al.* 2002, MNRAS, 335, L1
16. Fang, T., Davis, D. S., Lee, J. C., Marshall, H. M., Bryan, G. L., & Canizares, C. R. 2002, ApJ, 565, 86
17. Fabian, A. C., Rees, M. J., Stella, L., & White, N. E. 1989, MNRAS, 238, 729
18. Green, A., McHardy, I. M., & Lehto, H. J. 1993, MNRAS, 265, 664
19. Haardt, F., & Maraschi, L. 1991, ApJ, 380, L51
20. Haardt, F., & Maraschi, L. 1993, ApJ, 413, 507
21. Iwasawa, K., Fabian, A. C., Young, A. J., Inoue, H., & Matsumoto, C. 1999, MNRAS, 306, L19
22. Krolik, J. H., & Kallman, T. 1987, ApJ, 320, L5
23. Lee, J. C., Iwasawa, K., Houck, J. C., Fabian, A. C., Marshall, H. L., & Canizares, C. R. 2002, ApJ, 570, L47
24. Lubiński, P., & Zdziarski, A. A. 2001, MNRAS, 323, L37
25. Magdziarz, P., & Zdziarski, A. A. 1995, MNRAS, 273, 837
26. Markert, M., *et al.* 1995, Canizares, C. R., Dewey, D., McGuirk, M., Pak, C., & Shattenburg, M. L. 1995, *Proc. SPIE*, 2280, 168
27. Mathewson, D. S., & Ford, V. L. 1996, ApJS, 107, 97
28. Matt, G., Guainazzi, M., Perola, G. C., Fiore, F., Nicastro, F., Cappi, M., & Piro, L. 2001, A&A, 377, L31
29. Merloni, A., & Fabian, A. C. 2001, MNRAS, 328, 958
30. Nandra, K., George, I. M., Mushotzky, R. F., Turner, T. J., & Yaqoob, T. 1997, ApJ, 476, 70
31. Nandra, K., George, I. M., Turner, T. J., & Fukazawa, Y. 1996, ApJ, 464, 165
32. Nayakshin, S., & Kallman, T. 2001, ApJ, 546, 406
33. Nayakshin, S., & Kazanas, D. 2001, ApJ, 553, L141
34. Nayakshin, S., & Kazanas, D. 2002, ApJ, 567, 85
35. Netzer, H. 1990, in *Active Galactic Nuclei*, ed. R. D. Blandford, H. Netzer, & L. Woltjer (Berlin: Springer), 137
36. Oelgoetz, J., & Pradhan, A. K. 2001, MNRAS, 327, L42
37. Padovani, P., & Rafanelli, P. 1988, A&A, 205, 53
38. Perola, G. C., Matt, G., Cappi, M., Fiore, F., Guainazzi, M., Maraschi, L., Petrucci, P. O., & Piro, L. 2002, A&A, 389, 802
39. Petrucci, P. O., *et al.* 2002, A&A, 388, L5
40. Pike, C. D., *et al.* 1996, ApJ, 464, 487
41. Pounds, K. A., Reeves, J., O'Brien, P., Page, K., Turner, M. J.-L., & Nayakshin, S. 2001, ApJ, 559, 181
42. Pounds, K. A., Reeves, J. N., King, A. R., Page, K. L., O'Brien, P. T., & Turner, M. J. L. 2003, MN, submitted (astro-ph/0303603)
43. Reeves, J. N. 2002, in *ASP Conf. Ser., Active Galactic Nuclei, from Central Engine to Host Galaxy*, ed. S. Collin, F. Combes & I. Shlosman, (San Francisco: ASP), (astro-ph/0211381)
44. Reeves, J. N., Turner, M. J.-L., Pounds, K. A., O'Brien, P., Boller, Th., Ferrando, P., Kendziorra, E., & Vercellone, S. 2001, A&A, 365, L116
45. Reynolds, C. S., & Nowak, M. A. 2003, *Pys. Rep.*, in press (astro-ph/0212065)
46. Schulz, H., Knake, A., & Schmidt-Kaler, Th. 1994, A&A, 288, 425
47. Shull, J. M., & van Steenberg, M. 1982, ApJS, 48, 95
48. Shih, D. C., Iwasawa, K., & Fabian, A. C. 2002, MNRAS, 333, 687

48. Sulentic, J. W., Marziani, P., Zwitter, T., Calvani, M., & Dultzin-Hacyan, D. 1998, *ApJ*, 501, 54
49. Svensson, R., & Zdziarski, A. A. 1994, *ApJ*, 436, 599
50. Turner, T. J. 1987, *MNRAS*, 226, L9
51. Turner, T. J., George, I. M., & Nandra, K. 1998, *ApJ*, 508, 2
52. Turner, T. J., George, I. M., Nandra, K., & Turcan, D. 1999, *ApJ*, 524, 667
53. Turner, T. J., Romano, P., George, I. M., Edelson, R., Collier, S. J., Mathur, S., & Peterson, B. M. 2001, *ApJ*, 561, 131
54. Turner, T. J., *et al.* 2002, *ApJ*, 574, L123
55. Verner, D. A., Verner, E. M., & Ferland, G. J. 1996, *Atomic Data Nucl. Data Tables*, 64, 1
56. Weaver, K. A., Gelbord, J., & Yaqoob, T. 2001, *ApJ*, 550, 261
57. Weaver, K. A., Krolik, J. H., & Pier, E. A. 1998, *ApJ*, 498, 213
58. Yaqoob, T. 2001, in *ASP Conf. Ser., New Century of X-ray Astronomy*, ed. H. Inoue, & H. Kunieda (astro-ph/0108032)
59. Yaqoob, T., George, I. M., Nandra, K., Turner, T. J., Serlemitsos, P. J., & Mushotzky, R. F. 2001, *ApJ*, 546, 759
60. Yaqoob, T., McKernan, B., Done, C., Serlemitsos, P. J., & Weaver, K. A. 1993, *ApJ*, 416, L5
61. Yaqoob, T., McKernan, B., Kraemer, S. B., Crenshaw, D. M., Gabel, J. R., George, I. M., & Turner, T. J. 2003, *ApJ*, 582, 105
62. Yaqoob, T., & Padmanabhan, U. 2003, *High Resolution X-ray Spectroscopy with XMM-Newton and Chandra*, ed. G. Branduardi-Raymont, published electronically, http://www.mssl.ucl.ac.uk/~gbr/rgs_workshop/papers/yaqoob_t.ps
63. Yaqoob, T., Padmanabhan, U., Dotani, T., & Nandra, K. 2002, *ApJ*, 589, 487
64. Yaqoob, T., & Serlemitsos, P. J. 2000, *ApJ*, 544, L95
65. Yaqoob, T., Serlemitsos, P. J., Turner, T. J., George, I. M., & Nandra, K. 1996, *ApJ*, 470, L27
66. Zheng, W., Sulentic, J. W., & Binette, L. 1990, *ApJ*, 365, 115

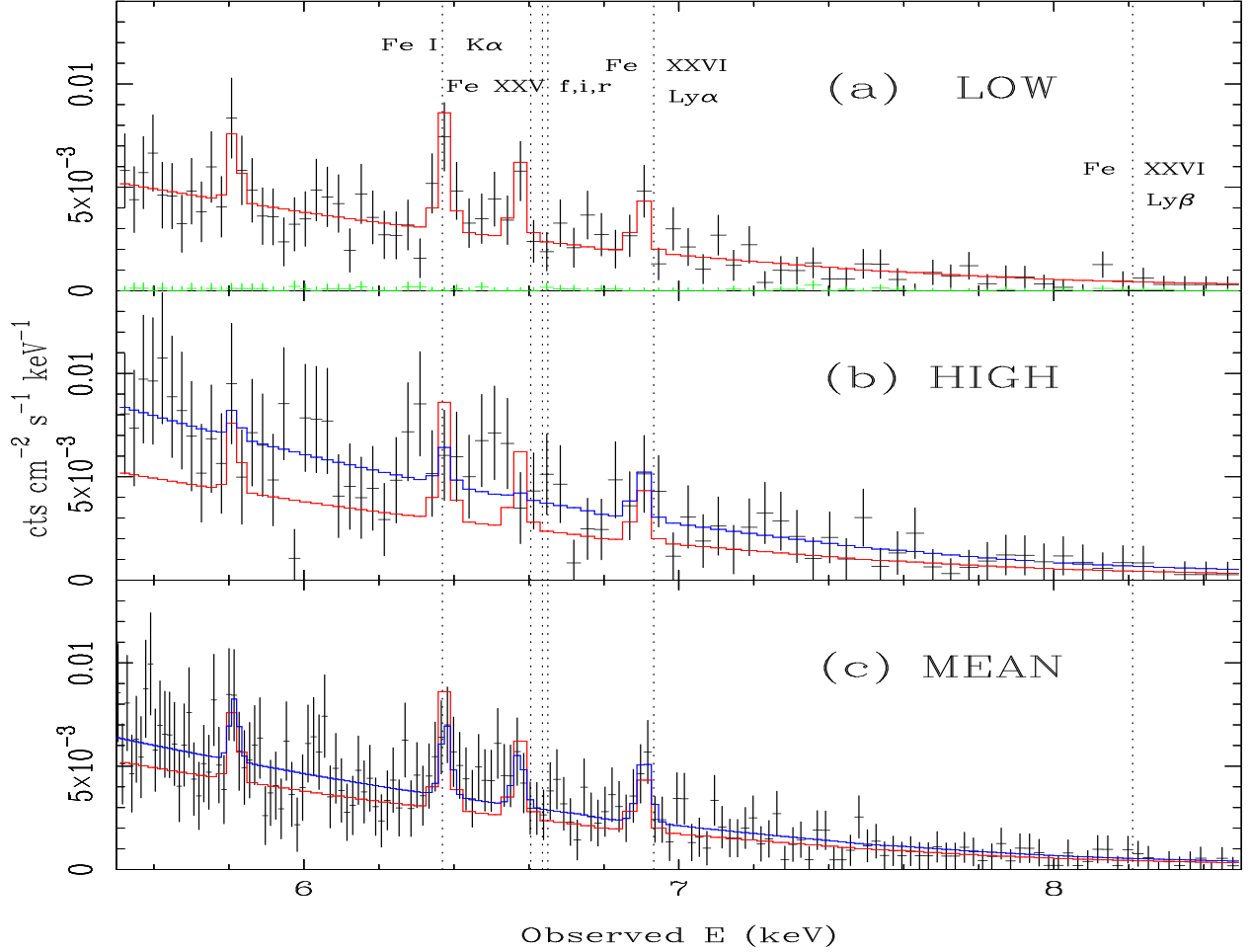


Figure 2. *Chandra* HEG low-state, high-state, and mean spectra in the 5.5–8.5 keV band. The bin size for the low-state and high-state spectra is 0.01\AA but 0.005\AA for the mean spectrum (the HEG FWHM resolution is 0.012\AA). The spectra have not been corrected for instrument response so that no artificially ‘sharp’ features are introduced into the plot: instead the models have been folded through the instrument response. The red solid lines in each panel corresponding to the best-fitting power-law plus four-Gaussian model to the *low-state* spectrum. The blue solid lines are the best-fitting models for the data shown in the appropriate panel (i.e. high-state and mean spectra). The normalized background spectrum extracted from a region 3.6–10 arcsec either side of the dispersion axis is shown in green in panel (a). In the low state we detect emission lines from Fe I–Fe XVII $K\alpha$, Fe XXV (f), Fe XXVI $\text{Ly}\alpha$, and Fe XXVI $\text{Ly}\beta$. The dotted lines show expected energies in the observer’s frame and it can be seen that the latter three lines are redshifted relative to the systemic velocity (see §3). None of the four emission lines modeled are resolved. In the high state the continuum has increased by a factor ~ 1.7 compared to the low state. In the high state, additional Fe $K\alpha$ emission appears redward of the energy of Fe I $K\alpha$, as well as some unresolved Fe $K\alpha$ emission from ionization intermediate between Fe I $K\alpha$ and Fe XXV. This response to the continuum is rapid (< 12.5 ks). See also Fig. 3. The emission line at 5.84 keV (rest-frame) remains unidentified, but could be due relativistically shifted Fe $K\alpha$ emission (see §4.2.1).

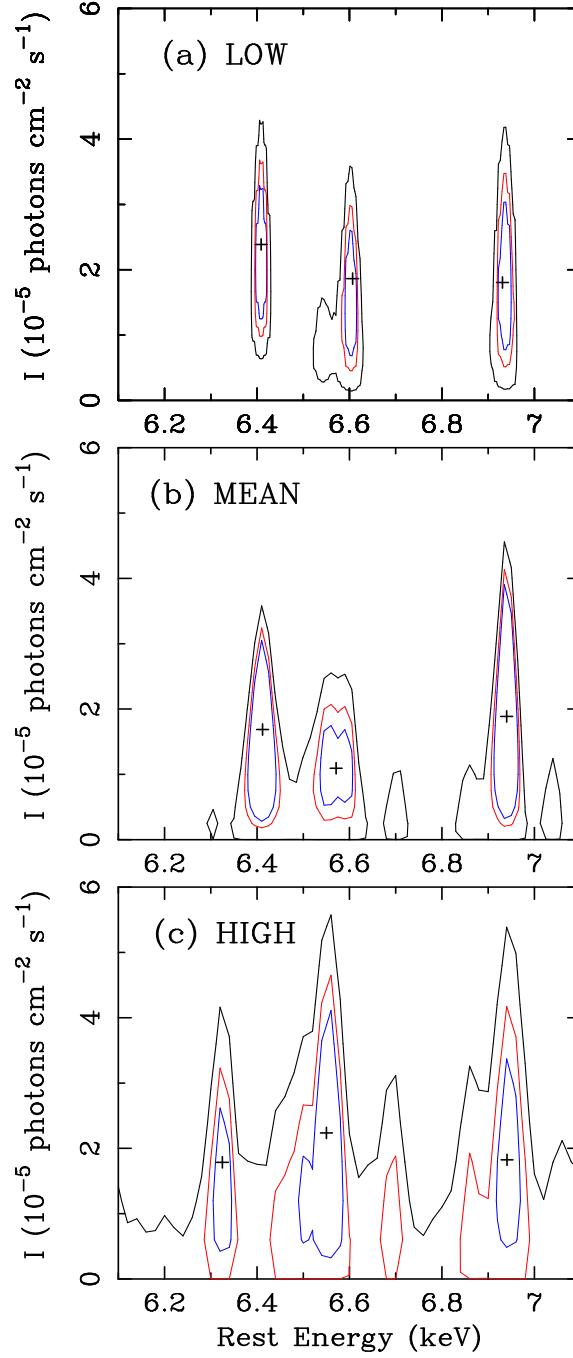


Figure 3. Confidence contours of line intensity versus energy, showing the rapid (< 12.5 ks) variability of the Fe-K emission complex in NGC 7314 (see also Fig. 2). The two-parameter joint confidence levels correspond to 68% (blue), 90% (red), and 99% (black). In the low state there are three clear, discrete emission features corresponding to $K\alpha$ line emission from Fe I–Fe XVII, Fe XXV, and Fe XXVI. Note that the signal-to-noise of the low-state and high-state spectra is approximately the same and the signal-to-noise of the mean spectrum is approximately twice that of either low-state or high-state spectra alone. Therefore the differences between the contours in different states are *not* due to signal-to-noise effects. This is supported by the fact that the centroid and width of the emission near 6.6 keV varies significantly (this is clearest from a comparison of the low-state and mean spectra). As the continuum level increases, the ionization structure of the emitting region changes from producing three discrete Fe $K\alpha$ features to a more complex blend of emission. In the high state, it also appears that the Fe XXVI Ly α emission becomes broader, and even the lowest ionization emission component appears to be variable: a peak below 6.4 keV becomes more prominent than the peak at ~ 6.4 keV.

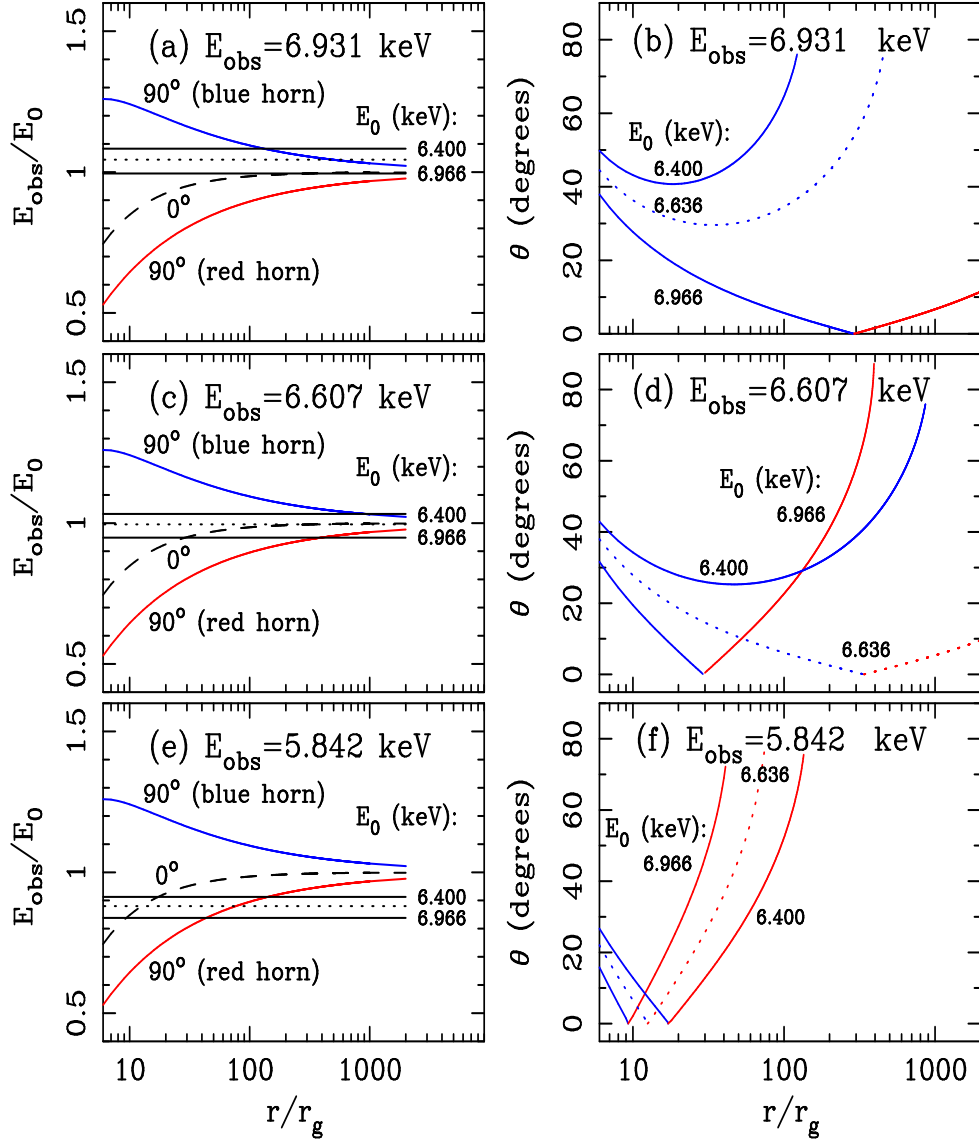


Figure 4. Constraints on the disk inclination angle (θ) and the radius (in units of $r_g \equiv GM/c^2$) from Fe $K\alpha$ emission lines originating from hot spots or annuli on a Keplerian disk rotating around a central Schwarzschild black hole (see §4.2). Pairs of panels are shown for each of the three strongest narrow lines observed in the low-state spectrum of NGC 7314, at observed energies (E_{obs}) of 6.931, 6.607, and 5.842 keV. Horizontal lines in panels (a), (c), and (e), and the curves in (b), (d), and (f) are labeled according to values of the line rest energy, E_0 , of 6.400 (Fe I $K\alpha$), 6.636 (Fe xxv (f): dotted), and 6.966 keV (Fe xxvi $\text{Ly}\alpha$). Blue curves indicate approaching parts of the disk and red curves indicate receding parts. For a given disk inclination angle, there are a pair of curves (blue and red) of E_{obs}/E_0 versus r/r_g , lying inside the 90° envelopes in panels (a), (c), and (e). The observed value of E_{obs}/E_0 would then vary (as a hot spot rotates with the disk) along a vertical line placed at a value of r/r_g corresponding to its location on the disk, between the appropriate blue and red curves. An annulus of emission, in which the observed lines are identified with either the red or blue Doppler horns, occupies a unique point in panels (a), (c), and (e), with specific values of θ , r/r_g , and E_{obs}/E_0 (if two of these quantities are known, there is no choice for the third). If the observed emission lines do indeed correspond to red or blue Doppler horns, panels (b), (d), and (f) show the necessary relations between θ and r/r_g for three values of E_0 .

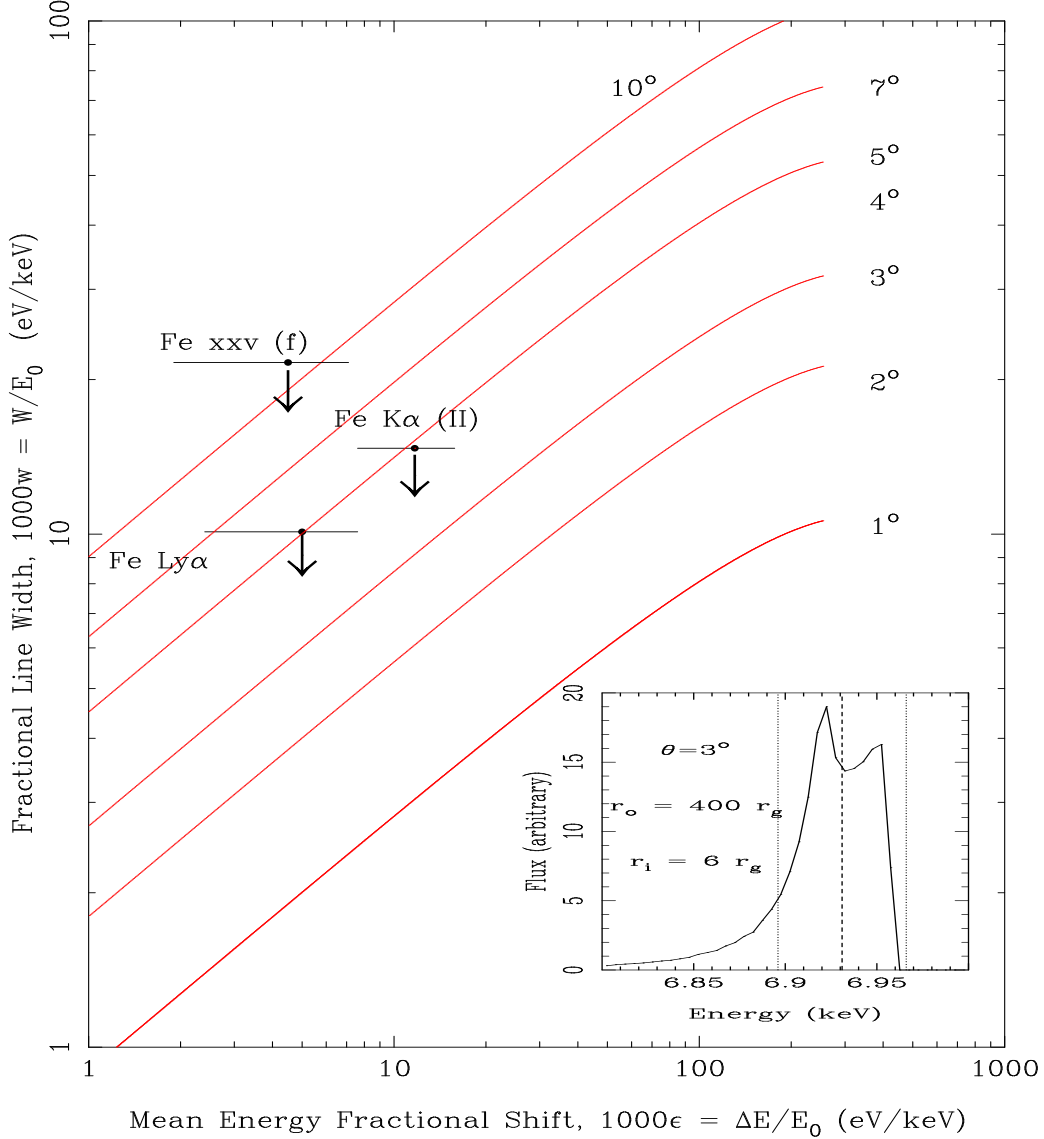


Figure 5. The relation between the minimum width ($w \equiv W_{\min}/E_0$), and energy shift ($\epsilon \equiv \Delta E/E_0$) of a monochromatic emission line (rest-energy, E_0), originating in a Keplerian disk rotating around a Schwarzschild black hole, for the case that the red and blue Doppler horns are unresolved (see §4.3). Plotted is $1000w$ versus 1000ϵ , for several inclination angles (solid lines). Note that, due to gravitational redshifting, the line centroid can never be blueshifted relative to the rest-energy. Each curve goes from 10^4 to 6 gravitational radii, from left to right, respectively. An emission line resulting from integration between *any two radii* on a disk with a given inclination angle must have measured widths and energy shifts (relative to the rest-energy) which lie *above* the curve for that inclination angle. The measurement of the upper limit on the width of Fe XXVI Ly α alone (it is unresolved) is firm enough to immediately rule out disks with $\theta > 7^\circ$ since the measurements do not lie above curves with $\theta > 7^\circ$. The Fe XXV (f) line is also consistent with $\theta < 7^\circ$. The implied maximum radius of emission (inferred from the Fe XXVI Ly α line) is $\sim 600r_g$. Also shown (inset) is the line profile expected if the Fe XXVI Ly α line were emitted uniformly (constant intensity per unit area) between 6 and 400 gravitational radii from a disk inclined at 3° . The dashed line shows the line centroid (as estimated simply from the mean energy of the two Doppler peaks), and the dotted line shows the FWHM upper limit measured from the low-state spectrum (see Table 1). The energy of the monochromatic model line is 6.966 keV in the disk frame, and the observed centroid of the relativistic line profile agrees with the measured centroid energy of 6.93 keV in the low state (see Table 1).

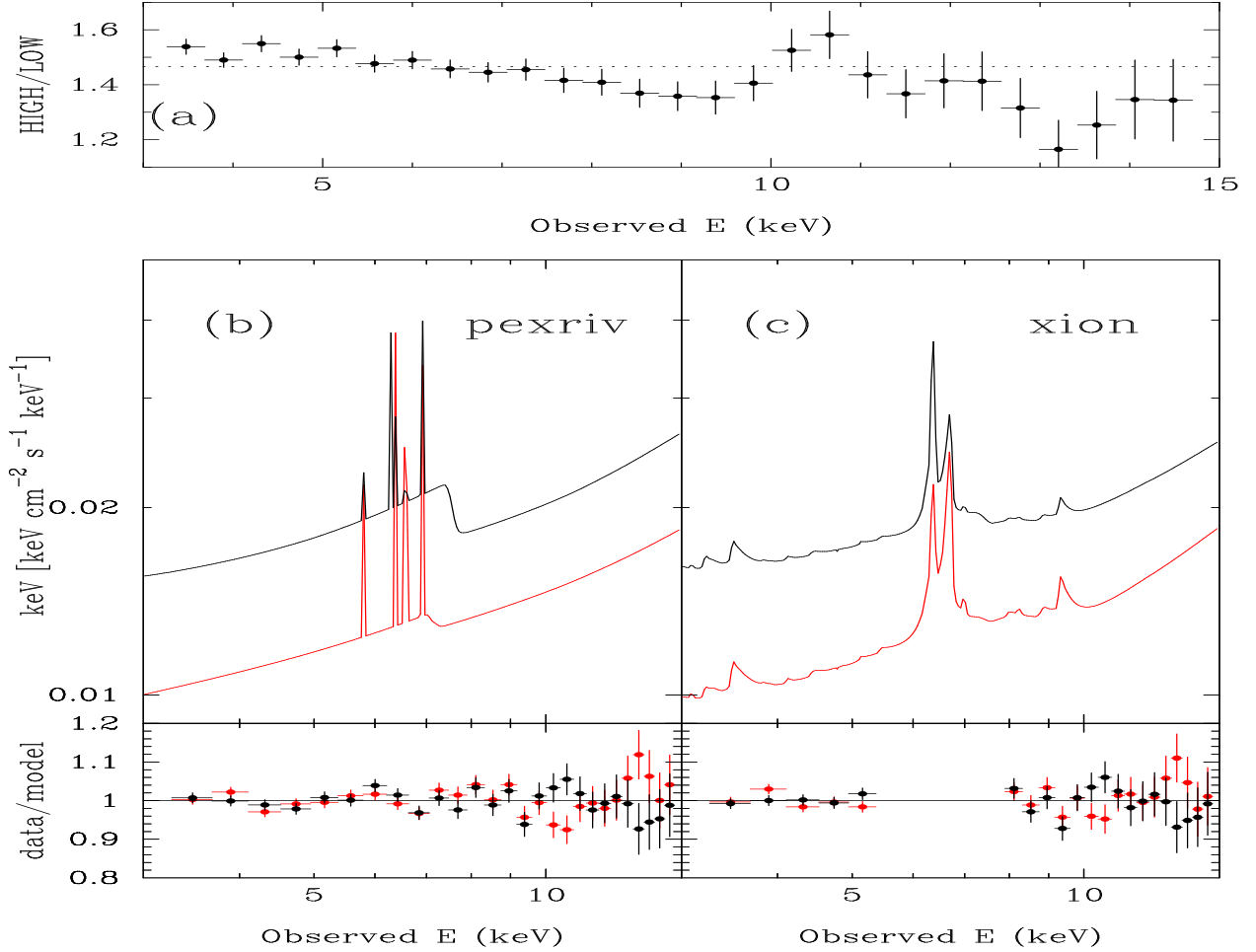


Figure 6. Results of time-resolved spectroscopy using the *RXTE* PCA data (combining PCU0 and PCU2). Details in §5. (a) Ratio of 3–15 keV high-state spectrum to low-state background-subtracted PCA spectra. The dotted line corresponds to the ratio of high-state to low-state 3–15 keV background-subtracted count rates. (b) Best-fitting ionized disk reflection models to the low-state (red) and high-state (black) PCA spectra, using the XSPEC model PEXRIV (Magdziarz & Zdziarski 1995). The Gaussian emission-line components were frozen at the best-fitting *Chandra* values (Table 1), corrected for the systematic difference in *Chandra* HEG and *RXTE* PCA normalizations (see §2.1). The lower panel shows the corresponding data/model ratios. (c) Best-fitting ionized disk reflection models to the low-state (red) and high-state (black) PCA spectra, using the XSPEC model XION (Nayakshin & Kallman 2001). The 5.5–7.5 keV data were omitted in the fits since the model does not allow disk inclination angles $< 18^\circ$ and does not include the effects of turbulence so predicts emission from H-like Fe to be much weaker than that from He-like Fe (we observe similar equivalent widths for both – see Fig. 2 and Table 1). The best-fitting models illustrate the line emission predicted by XION (relativistic smearing was turned off for the plot in order to show clearly the relative strengths of the lines from different ionization states).

Table 1
Chandra HEG Spectral Fitting Results

Parameter	Low State (I) ^a	Low State (II) ^a	Mean	High State
<i>C</i> (degrees of freedom)	117.7 (99)	118.7(100)	236.9/(211)	116.6/(103)
Fe Kα (I) ^b				
<i>E</i> ₀ (keV)	6.405 ^{+0.016} _{-0.017}	6.405 ^{+0.016} _{-0.017}	6.412 ^{+0.010} _{-0.016}	fixed (6.405)
1 - (<i>E</i> ₀ /6.400)	-0.8 ^{+2.7} _{-2.5} × 10 ⁻³	-0.8 ^{+2.7} _{-2.5} × 10 ⁻³	-1.9 ^{+2.5} _{-1.6} × 10 ⁻³	...
<i>c</i> ΔE /6.400 (km s ⁻¹)	-240 ⁺⁸¹⁰ ₋₇₅₀	-240 ⁺⁸¹⁰ ₋₇₅₀	-570 ⁺⁷⁵⁰ ₋₄₈₀	...
σ (keV)	< 0.032	< 0.032
FWHM (km s ⁻¹)	< 3520	< 3520
<i>I</i> (10 ⁻⁵ photons cm ⁻² s ⁻¹)	2.4 ^{+1.0} _{-1.0}	2.5 ^{+0.9} _{-1.1}	1.7 ^{+0.7} _{-0.8}	0.8 ^{+1.3} _{-0.8}
EW (eV)	81 ⁺³⁴ ₋₃₄	83 ⁺³⁰ ₋₃₇	48 ⁺²⁰ ₋₂₃	18 ⁺²⁹ ₋₁₈
Fe Kα (II) ^b				
ΔC ^c	0.0	-0.3	-0.2	-6.5
<i>E</i> ₀ (keV)	fixed (6.325)	fixed (6.325)	fixed (6.325)	6.325 ^{+0.026} _{-0.014}
1 - (<i>E</i> ₀ /6.400)	1.17 ^{+0.22} _{-0.41} × 10 ⁻²
<i>c</i> ΔE /6.400 (km s ⁻¹)	3510 ⁺⁶⁶⁰ ₋₁₂₃₀
σ (keV)	< 0.040
FWHM (km s ⁻¹)	< 4460
<i>I</i> (10 ⁻⁵ photons cm ⁻² s ⁻¹)	< 0.3	< 0.3	< 0.7	1.8 ^{+1.5} _{-1.3}
EW (eV)	< 7	< 7	< 15	39 ⁺³³ ₋₂₈
Fe xxv (f)				
<i>E</i> ₀ (keV)	6.607 ^{+0.011} _{-0.017}	6.607 ^{+0.011} _{-0.017}	fixed (6.607)	fixed (6.607)
1 - (<i>E</i> ₀ /6.637)	4.5 ^{+2.6} _{-1.7} × 10 ⁻³	4.5 ^{+2.6} _{-1.7} × 10 ⁻³
<i>c</i> ΔE /6.637 (km s ⁻¹)	1350 ⁺⁷⁸⁰ ₋₅₁₀	1350 ⁺⁷⁸⁰ ₋₅₁₀
σ (keV)	< 0.061	< 0.061
FWHM (km s ⁻¹)	< 6510	< 6510
<i>I</i> (10 ⁻⁵ photons cm ⁻² s ⁻¹)	1.9 ^{+0.8} _{-1.1}	1.9 ^{+0.8} _{-1.1}	1.1 ^{+0.7} _{-0.6}	0.2 ^{+1.3} _{-0.2}
EW (eV)	59 ⁺²⁵ ₋₃₄	60 ⁺²⁵ ₋₃₅	29 ⁺²⁰ ₋₁₇	3 ⁺²⁸ ₋₃
Fe xxvi Lyα				
<i>E</i> ₀ (keV)	6.931 ^{+0.018} _{-0.011}	6.931 ^{+0.018} _{-0.011}	6.940 ^{+0.010} _{-0.010}	fixed (6.931)
1 - (<i>E</i> ₀ /6.966)	5.0 ^{+1.6} _{-2.6} × 10 ⁻³	5.0 ^{+1.6} _{-2.6} × 10 ⁻³	3.7 ^{+1.5} _{-1.4} × 10 ⁻³	...
<i>c</i> ΔE /6.966 (km s ⁻¹)	1500 ⁺⁴⁸⁰ ₋₇₈₀	1500 ⁺⁴⁸⁰ ₋₇₈₀	1110 ⁺⁴⁵⁰ ₋₄₂₀	...
σ (keV)	< 0.030	< 0.030	< 0.026	< 0.101
FWHM (km s ⁻¹)	< 3050	< 3050	< 2640	< 10270
<i>I</i> (10 ⁻⁵ photons cm ⁻² s ⁻¹)	1.8 ^{+1.4} _{-0.8}	1.9 ^{+1.4} _{-0.8}	1.9 ^{+1.0} _{-0.7}	1.7 ^{+1.8} _{-1.2}
EW (eV)	68 ⁺⁵³ ₋₃₀	71 ⁺⁵³ ₋₃₀	63 ⁺³³ ₋₂₃	44 ⁺⁴⁷ ₋₃₁

Table 1
–Continued

Parameter	Low State (I) ^a	Low State (II) ^a	Mean	High State
Unidentified				
E_0 (keV)	$5.842^{+0.12}_{-0.14}$	$5.842^{+0.12}_{-0.14}$	fixed (5.842)	fixed (5.842)
σ (keV)	< 0.030	< 0.030
FWHM (km s ⁻¹)	< 3620	< 3620
I (10 ⁻⁵ photons cm ⁻² s ⁻¹)	$1.0^{+2.0}_{-0.5}$	$1.0^{+2.0}_{-0.5}$	$0.7^{+0.6}_{-0.5}$	$0.4^{+1.0}_{-0.4}$
EW (eV)	32^{+64}_{-16}	32^{+64}_{-16}	19^{+16}_{-14}	8^{+20}_{-8}
F(2–10 keV) ^d	2.5	2.5	3.0	4.0
L(2–10 keV) ^e	1.2	1.2	1.5	2.0

Gaussian modeling of the emission lines in the NGC 7314 HEG data (see §3). The baseline model has four Gaussians (see Fig. 2 and §3). The intrinsic width of each Gaussian is fixed at 1 eV, but allowed to float in turn to determine the upper limit (temporarily freezing the line energy in the process). Statistical errors and upper limits are for 90% confidence ($\Delta C = 2.706$). All emission-line parameters refer to the rest-frame of NGC 7314 ($z = 0.004760$). Velocities have been rounded to the nearest 10 km s⁻¹.

^a All except the low-state (II) results refer to fits with a simple power law for the continuum fitted in the 5–9 keV range. To demonstrate the robustness to details of how the continuum is modeled, the low-state (II) results are obtained by fitting the continuum with an absorbed power law in the 0.8–9 keV band. See §3 for details.

^b Two distinct Fe K α components are detected. Fe K α (I) is not variable and is not redshifted relative to 6.400 keV and is therefore a ‘distant-matter’ component. Fe K α (II) is variable and is redshifted relative to 6.400 keV.

^c Change in C -statistic when the Fe K α (II) component is added to the four-Gaussian model.

^d Observed flux in units of 10⁻¹¹ ergs cm⁻² s⁻¹.

^e Intrinsic luminosity in the source frame, in units of 10⁴² ergs s⁻¹, assuming $H_0 = 70$ km s⁻¹ Mpc⁻¹, and $q_0 = 0$.

Table 2
RXTE PCA Spectral Fitting Results

Model ^a	Parameter	Low State	High State
Power Law	χ^2 /(degrees of freedom)	48.2/25	90.9/25
PEXRAV ^b	χ^2 /(degrees of freedom)	38.4/24	67.1/24
Power Law & Edge	χ^2 /(degrees of freedom)	41.9/23	35.2/23
PEXRAV ^b & Edge	χ^2 /(degrees of freedom)	31.5/22	32.9/22
	Γ	$1.73^{+0.08}_{-0.07}$	$1.59^{+0.12}_{-0.04}$
	R (Reflection Fraction)	$1.03^{+0.59}_{-0.47}$	$0.02^{+0.60}_{-0.02}$
	Edge Energy (keV)	$9.53^{+0.60}_{-0.63}$	$7.97^{+0.36}_{-0.23}$
	$\tau_{\text{threshold}}$	$0.088^{+0.059}_{-0.055}$	$0.222^{+0.056}_{-0.063}$
PEXRIV ^b	χ^2 /(degrees of freedom)	39.3/22	26.2/22
	Γ	$1.73^{+0.07}_{-0.07}$	$1.88^{+0.09}_{-0.07}$
	R (Reflection Fraction)	$0.71^{+0.44}_{-0.36}$	$1.23^{+0.62}_{-0.41}$
	T_{disk} (Kelvin)	$(10^4-10^6)^d$	$> 1.2 \times 10^5$
	ξ (erg cm s ⁻¹)	0.02 (< 56)	27^{+62}_{-15}
XION ^c	χ^2 /(degrees of freedom)	21.6/17	15.5/17
	Γ	$1.72^{+0.06}_{-0.05}$	$1.90^{+0.06}_{-0.08}$
	L_X/L_{disk}	0.02 (< 0.42)	0.05 (< 4.5)
	$\dot{m}/\dot{m}_{\text{Edd}}$	0.49 (> 0.27)	0.07 (< 0.36)
		OR 0.02–0.15 ^e	

Spectral fits were performed in the 3–15 keV band. Details of the fits in §5 (see also Fig. 6). Statistical errors are quoted for 90% confidence, 1 interesting parameter ($\Delta\chi^2 + 2.706$).

^a Gaussian emission lines were included (except for the XION model), with parameter values frozen at the best-fitting low-state and high-state *Chandra* HEG values (Table 1), corrected for HEG/PCA cross-normalization difference (see §2.1).

^b PEXRAV and PEXRIV are ‘cold’ and ionized disk-reflection models respectively, due to Magdziarz & Zdziarski (1995). These models produce only continuum, no lines.

^c XION: ionized disk reflection model due to Nayakshin & Kallman (2001). XION does not allow disk inclination angles < 18° and predicts Fe XXV line emission to be much stronger than that from Fe XXVI (Fig. 6), but the two lines are observed to have about the same EW (Fig. 2). Therefore we omitted the 5.5–7.5 keV regions of the PCA spectra.

^d No constraint on the disk temperature was obtained in the given range.

^e 90% confidence range of a second solution for $\dot{m}/\dot{m}_{\text{Edd}}$ in the low state.